Fakultät für Medizin

Friedrich-Schiedel Institut für Neurowissenschaften

Cellular mechanisms of visual processing in the mammalian brain

Yang Chen

Vollständiger Abdruck der von der Fakultät für Medizin der Technischen Universität München zur Erlangung des akademischen Grades eines

Doctor of Philosophy (Ph.D.)

genehmigten Dissertation.

Vorsitzende/r: Univ.-Prof. Dr. Claus Zimmer

Betreuer/in: Univ.-Prof. Dr. Arthur Konnerth

Prüfer der Dissertation:

1. apl. Prof. Dr. Helmuth Adelsberger

2. Univ.-Prof. Dr. Markus Ploner

Die Dissertation wurde am 05.09.2017 bei der Fakultät für Medizin der Technischen Universität München eingereicht und durch die Fakultät für Medizin am 22.09.2017 angenommen.

Cellular mechanisms of visual processing in the mammalian brain

Abstract

In the canonical circuit of the mammalian visual cortex, visual information from the retina, through projections of the thalamic lateral geniculate nucleus (LGN), reaches layer 4 (L4) of the primary visual cortex (V1). This classical view on visual information processing was pioneered by the seminal work of Hubel & Wiesel, which established an influential model that orientation selectivity in V1 emerges at the information transfer from the LGN to L4. However, the generality of this model was challenged by recent findings in mice demonstrating that a large portion of orientation and direction selective neurons exist in the LGN. These findings implied the existence of alternative models for orientation selectivity, at least for the mouse visual system.

In the present study, we used new methodological developments to explore the cellular and circuit mechanisms of orientation selectivity in the mouse visual system. First, we performed two-photon calcium imaging of neuronal populations in L4 of the mouse V1 and identified highly responsive but orientation/direction selective neurons in L4 (super responsive neurons, SR neurons). These SR neurons represented a small fraction of L4 neurons (about 5%) and fired more than 20 action potentials per second in response to preferred stimulus direction. Next, we targeted the SR neurons for dendritic calcium imaging and electrophysiological recording to study their apical tuft dendrites. Interestingly, these dendrites generated reliable dendritic calcium spikes to the preferred direction of drifting gratings. The dendritic calcium spikes were proved to be NMDA receptor-dependent and required tuned synaptic inputs in layer 1. Furthermore, they correlated with high frequency somatic action potentials and contributed substantially to the output of SR neurons.

In conclusion, our study revealed an important role of active apical tuft dendrites in visual processing in L4 of mouse V1 and provided new insights in cortical computation.

Zelluläre Mechanismen der Verarbeitung visueller Reize des Gehirns von Säugetieren

Zusammenfassung

Im weithin anerkannten neuronalen Schaltkreis des visuellen Kortex im Gehirn der Säugetiere, werden visuelle Informationen von der Retina, über den Corpus geniculatum laterale (LGN) des Thalamus, an die Neurone der Schicht 4 (L4) des primären visuellen Kortex weitergeleitet (V1). Diese klassische Sicht der Signalverarbeitung visueller Informationen wurde von den Pionieren Hubel & Wiesel eingeführt, die das maßgebende Model entwarfen, in dem Orientierungsselektivität im Signaltransfer zwischen LGN und Schicht 4 des Kortex aufkommt. Allerdings hält diese vereinfachte Sicht neuen Erkenntnissen der Forschung nicht stand, da orientierungs- und richtungsselekive Neuronen auch im LGN nachgewiesen wurden. Diese Erkenntnisse deuten darauf hin, dass es alternative Modelle der Entstehung von Orientierungsselektivität existieren müssen, zumindest im visuellen System der Maus.

Im Rahmen dieser Arbeit haben wir neue technische Entwicklungen angewandt, um zelluläre und Netzwerk-Mechanismen der Orientierungsselektivität einzelner Neurone des visuellen Systems der Maus nachzuvollziehen. Zuerst wurden Zwei-Photonen Kalziummessungen neuronaler Zellpopulationen in Schicht 4 des visuellen Kortex der Maus durchgeführt, wobei stark antwortende sowie orientierungs-/richtingsselektive Neuronen in Schicht 4 identifiziert wurden (“super-antwortende” Neuronen, SA Neuronen). Diese SA Neuronen stellen einen kleinen Anteil der Schicht 4 Neuronen dar (ca. 5%) und antworten mit mehr als 20 Aktionspotentialen pro Sekunde auf die bevorzugte Richtung des visuellen Stimulus. Um gezielt die Tuftdendriten dieser SA Neuronen zu untersuchen, wurden dendritische Kalziummesungen und elektrophysiologische Messungen dieser Zellen durchgeführt. Interessanterweise antworteten diese Dendriten zuverlässig mit dendritischen Kalziumspikes auf die bevorzugte Richtung des Bewegungsmusters. Es wurde gezeigt, dass die Kalziumspikes abhängig von NMDA-Rezeptoren sind und richtungsspezifische synaptische Inputs in Schicht 1 benötigen. Des Weiteren traten sie in Korrelation mit hochfrequenten somatischen Aktionspotentialen auf und trugen maßgeblich zu den Output-Signalen der SA Neuronen bei.

Zusammenfassend identifiziert unsere Studie die wichtige Bedeutung der aktiven apikalen Tuftdendriten im Hinblick auf die Verarbeitung visueller Informationen in Schicht 4 des primären visuellen Kortex der Maus auf und lieferte neue Erkenntnisse zur kortikalen Signalverarbeitung.

Table of Contents

Abbreviations

AAV	adeno-associated virus
AM	acetoxymethyl
AMPA	α-amino-3-hydroxy-5-methyl-4-isoxazolepropionic acid
AMPAR	AMPA receptor
AOD	acousto-optical deflector
AP	action potential
APV	D-(-)-2-Amino-5-phosphonopentanoic acid
bAP	back-propagating action potential
BPM	beat per minute
CC	current clamp mode
CNQX	6-Cyano-7-nitroquinoxaline-2,3-dione
dLGN	dorsal lateral geniculate nucleus
ΔF/F	normalized fluorescence change
GΩ	gigaohm
GYKI	4-(8-Methyl-9*H*-1,3-dioxolo[4,5-*h*][2,3]benzodiazepin-5-yl)-benzenamine dihydrochloride (GYKI 52466)
Hz	Hertz
Kd	dissociation constant
L1	layer 1
L4	layer 4
MCBL	multi-cell bolus loading
mm	millimeter
mM	millimolar

MΩ	megaohm
ms	millisecond
mV	millivolt
mW	milliwatt
µm	micrometer
nA	nanoampere
nm	nanometer
NMDA	N-Methyl-D-aspartic acid
NMDAR	NMDA receptor
OGB1	Oregon Green 488 BAPTA-1
OGB1-6k	Oregon Green 488 BAPTA-1 hexapotassium salt
RGCs	retinal ganglion cells
pA	picoampere
PBS	phosphate buffered saline
ROI	region of interest
SNR	signal-to-noise ratio
TTX	tetrodotoxin
V1	primary visual cortex
VC	voltage clamp mode
VGCC	voltage-gated Ca^{2+} channel

1 Introduction

A fundamental function of our brain is to process information. It collects sensory information from the outside world and makes decisions based on collected information. The sensory information processing capability of the brain attributes mostly to the neocortex. Neocortex contains six cellular layers, and inside each layer, there are different groups of neurons with distinct morphology, connectivity, and electrophysiological property. Among them, around 80% of neocortical neurons are excitatory principal neurons and most of them respond selectively to sensory stimuli. The rest 20% are inhibitory interneurons which mainly regulate local circuits. Cells within layers or across layers are interconnected to make up complex neocortical circuits which are the basis of sensory information processing.

The exploration of neocortical circuits dated back to the work of Santiago Ramón y Cajal a century ago. However, the understanding of sensory information processing in neocortex had been limited until the discovery of orientation selective receptive field of simple cells (Hubel and Wiesel, 1959) and a revolutionary model for the underlying mechanism (Hubel and Wiesel, 1962). In this model, the orientation tuned receptive field emerges from the arrangement of untuned thalamic inputs. Since then, visual cortex has served as a canonical model system for the study of neocortical circuits.

1.1 Mouse visual system

With the increasing knowledge of molecular biology and emergence of new genetical tools, mouse as an animal model to study neural system has become more and more popular. In particular, the creation of various Cre mouse lines enabled us to label and trace specific neuron types and circuits. The study of gene-related diseases became possible with the making of gene-specific knock-out mouse lines. These benefits of mice attracted many neuroscientists, particularly those from visual neuroscience. From the point of view of the 3Rs principles (Replacement, Reduction and Refinement), the mouse is also advantageous to cat and monkey. In this section, the mouse visual system will be briefly introduced. The emphasis here is on the main visual pathway (retina -> dLGN -> V1).

Our knowledge about visual system came mainly from the studies using cats and primates. For a long time, the mouse was not preferred as the subject to study visual system for several reasons. For instance, mice are nocturnal animals which prefer dark environment and avoid light. They rely mostly on auditory, tactile and olfactory cues to explore surrounding environment. Besides, their visual acuity is extremely low and their eyes are also too small to study.

The first quantification of responsive properties of neurons in the mouse visual cortex was done by Ursula Dräger in 1975 (Dräger and Drager, 1975). She identified that, in the mouse visual cortex, neurons have similar orientation and direction selective receptive fields to those in cat and monkey visual cortex. Later studies identified many similarities between mice and higher mammals regarding receptive field properties (Mangini and Pearlman, 1980; Metin et al., 1988) and retinotopic organizations (Wagor et al., 1980).

1.1.1 Architecture of the mouse visual system

The architecture of mouse visual system shares similarities with that of other vertebrates. It consists of several stations including eye, visual thalamus, visual cortex and so on. Inside each station, there are dedicated cells types and local neural circuits. These stations are linked together through long-range connections to form a hierarchical structure.

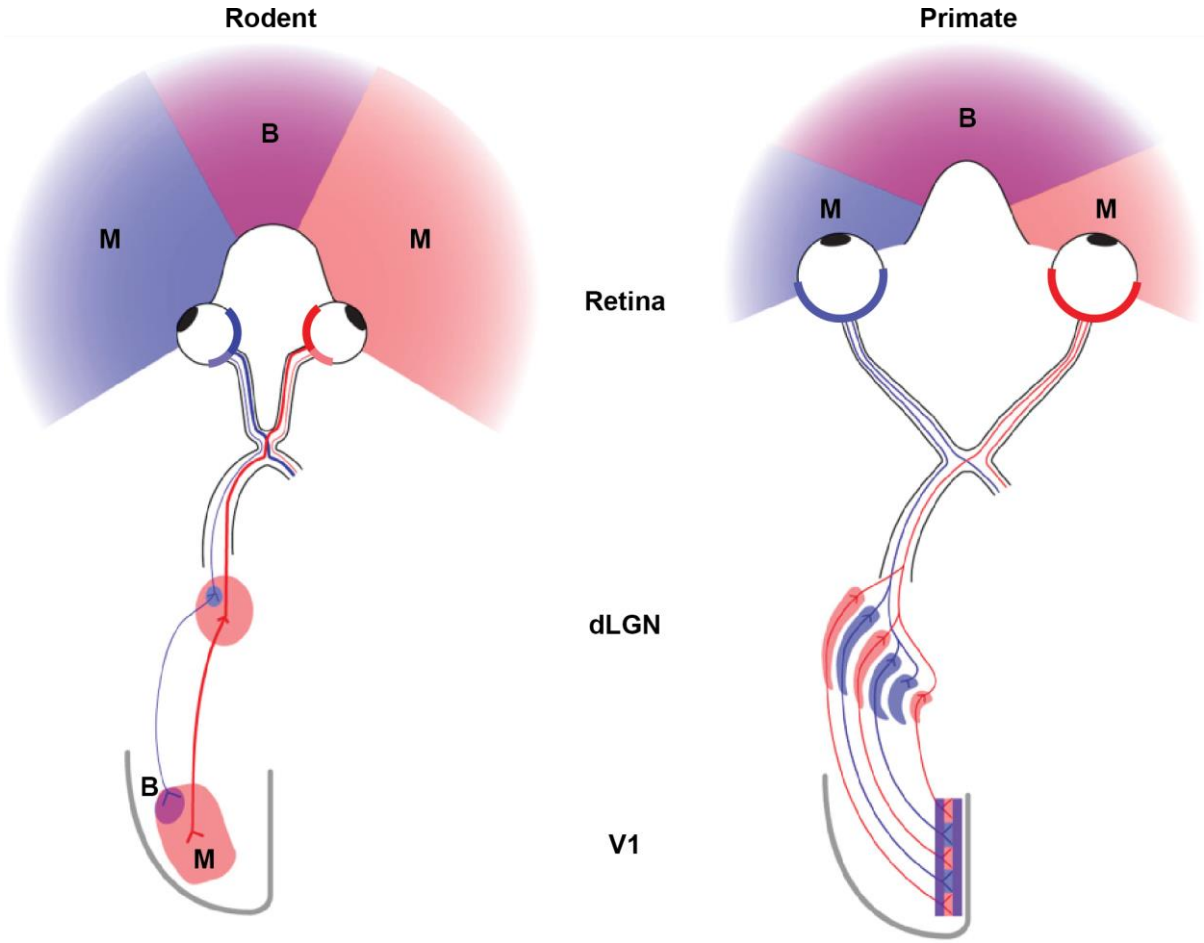

Fig. 1. Rodent and primate visual systems. Left, schematic of rodent visual system. Right, schematic of primate visual system. B, binocular area. M, monocular area. dLGN, dorsal lateral geniculate nucleus. V1, primary visual cortex. Diagram reproduced from (Priebe and McGee, 2014).

The retina is the first stage of visual information processing. The mouse retina does not have a fovea which accounts partly for its low visual acuity. Except for this, mouse retina shares a similar structure to other higher animals. The mouse retina has three major functionally different layers: the outer nuclear layer which contains photoreceptors; the inner nuclear layer which contains mostly interneurons; and the ganglion cell layer which contains retinal ganglion cells (RGCs). In the outer nuclear layer, both rods and cones photoreceptor are present and are distinct in number, distribution, and sensitivity. Their function is to convert light signals into electrical signals. The inner nuclear layer is where horizontal, bipolar, and amacrine cells reside. Horizontal cells form the link between different photoreceptors. Bipolar cells receive inputs from photoreceptors and target amacrine cells and ganglion cells. Amacrine cells are inhibitory neurons and usually form a local circuit between bipolar cells and

ganglion cells. These cells perform initial transformation of light-induced electrical signals. The ganglion cell layer is the output layer of the retina. RGCs integrate signals from bipolar cells and amacrine cells. The axons of RGCs leave retina and project to subcortical areas. More than 90% of the projections cross the optic chiasm to the contralateral side while the rest do not (Dräger, 1974; Valverde, 1968). Among those projected areas, dorsal lateral geniculate nucleus (dLGN) is the main target area which directly conveys visual information further to the visual cortex.

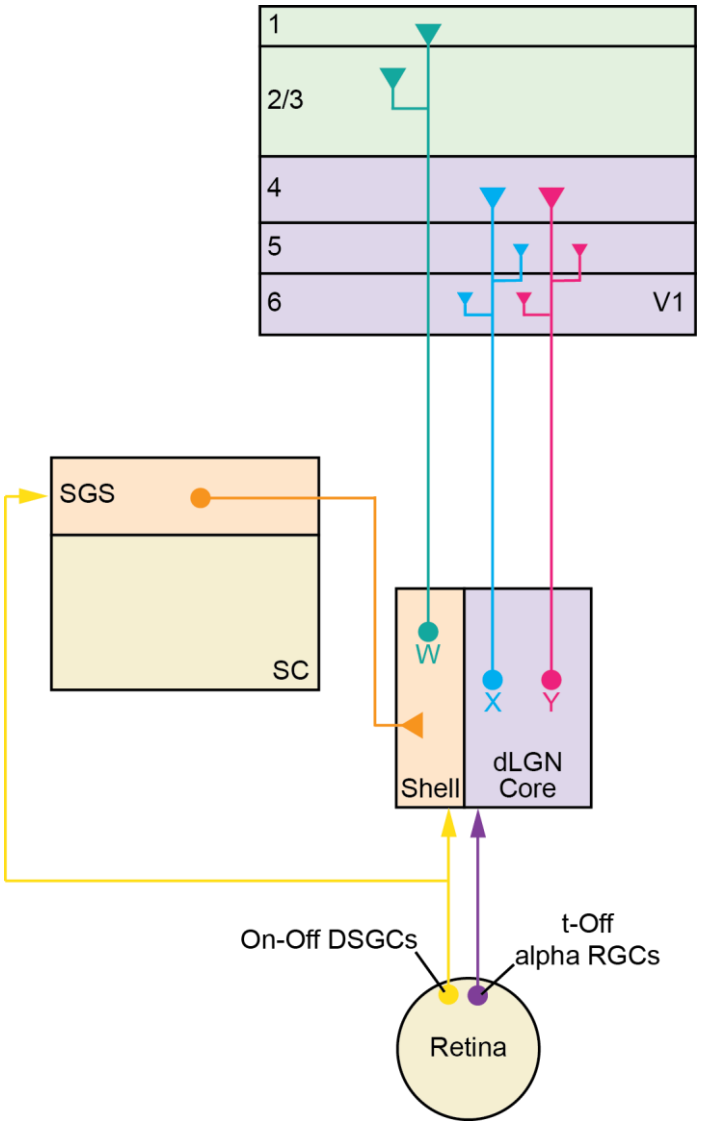

Fig. 2 Schematic pathways of mouse dLGN. DSGC, direction-selective ganglion cell. RGCs, retinal ganglion cells. t-Off, transient Off. dLGN, dorsal lateral geniculate nucleus. SC, superior colliculus. SGS, stratum griseum superficialis. V1, primary visual cortex. Scheme reproduced from (Seabrook et al., 2017).

The mouse dLGN does not have a laminar structure like primates in which different layers receive either ipsilateral or contralateral inputs (Fig. 1). The mouse dLGN can be further divided into the shell and the core regions, each of which projects to different layers of primary visual cortex. Inside dLGN, there are morphological distinct groups of thalamic relay cells. X-like (biconical) and Y-like (symmetrical) cells were mostly found in core region while W-like (hemispheric) cells mostly reside shell region (Krahe et al., 2011). X-like and Y-like cells receive inputs from non-direction-selective alpha RGCs (see later for RGC types) and project to layer 4 of V1. W-like cells receive inputs from On-Off and Off-direction selective RGCs (DSGCs) and project to layer 1 and layer 2/3 of V1 (Fig. 2) (Bickford et al., 2015; Cruz-Martín et al., 2014; Krahe et al., 2011).

The mouse visual cortex sits at the occipital part of the brain and has the same 6-layer structure as other higher animals. It is composed of primary visual cortex (V1) and surrounding higher visual areas. V1 is the major cortical area receiving inputs from dLGN. In contrast to previous knowledge that V1 receives dLGN inputs only in layer 4, there is increasing evidence that dLGN terminals target several V1 layers (Bickford et al., 2015; Cruz-Martín et al., 2014; Kondo and Ohki, 2015; Sun et al., 2015). V1 can be divided into the medially located monocular zone and the laterally located binocular zone. As the name suggests, the monocular zone receives visual inputs only from the contralateral eye and the binocular zone receive inputs from bilateral eyes. The mouse V1 has the same 6-layer structure as other higher animals. Interestingly, neurons in layer 4 of mouse V1 have a pyramidal morphology (star pyramidal neurons) with long apical dendrites spanning several layers, which is in sharp contrast to V1 of cat and monkey where neurons are mostly stellate cells with dendrites restricting largely in layer 4. Considering the distribution of dLGN terminals in different layers of mouse V1, neurons in layer 4 of mouse V1 could potentially integrate dLGN inputs of multiple sources on different dendritic compartments.

1.1.2 Responsive properties of mouse visual system

In every station of the mouse visual system, most neurons inside show certain responses to external visual stimuli. Those responses reflect the computation being performed inside individual neurons and in the local circuit. By looking at the response

properties of cells in each station, we can get a rough idea of how visual information is processed and conveyed along the pathway in the visual system.

In the mouse retina, photoreceptors are responsible for light detection and signal conversion from photon to electrical signals. They respond not to a detailed specific feature of visual stimuli, but to the general properties of light, for example, wavelength and intensity. Wavelength preference of rod photoreceptors in the mouse retina is 497-500 nm green light (Fan et al., 2005). In contrast, most cone photoreceptors respond best to 360 nm UV light, but the ones in the dorsal part of retina prefer 508 nm green light (Nikonov et al., 2006; Szél et al., 1992, 1993). RGCs in the mouse retina can be classified into many types based on function and morphology. A conventional type is alpha ganglion cell which could exhibit responses like sustained On, sustained Off, and transient Off (van Wyk et al., 2009). Another type of ganglion cells is direction selective ganglion cell (DSGC), which has direction preference. DSGCs are further divided into On, Off and On-Off subtypes depend on their response pattern. DSGCs get their response properties through a subtype of amacrine cells (starburst amacrine cells) (Vaney et al., 2012; Vlasits et al., 2014).

In the mouse dLGN, cells were thought to have circular receptive fields (On and Off centers) as other species, and it was confirmed by an early study (Grubb and Thompson, 2003). However, recent studies also revealed the existence of a substantial amount (10%-40%) of orientation selective (OS) and direction selective (DS) cells (Marshel et al., 2012; Piscopo et al., 2013; Scholl et al., 2013; Zhao et al., 2013). These OS and DS cells particularly concentrated in the shell region of dLGN which is one of the main targeting areas of DSGCs (Rivlin-Etzion et al., 2011).

Responses of neurons in mouse V1 are layer dependent. Early studies (Mangini and Pearlman, 1980; Metin et al., 1988) showed that neurons with a less orientation selective, circular receptive field (On, Off, and On-Off centers) were largely found in layer 4 and OS neurons were more frequent in layer 2/3. Layer 5 contained neurons with a large and non-orientated receptive field. Those findings of early studies showed mouse V1 neurons to be less selective than that of other animals because of technical limitations. However, more recent studies demonstrated a much higher degree of selectivity of mouse V1 neurons in all layers which is comparable to other species. Other response properties like linear, nonlinear spatial summation and contras-

invariant tuning were also found in V1. In particular, inhibitory interneurons were shown to be less tuned and nonlinear (Liu et al., 2009; Niell and Stryker, 2008). It is important to note that there is a huge difference in V1 between mouse and higher mammals. Orientation selective neurons in mouse V1 do not organize into a columnar structure like cats and monkeys and instead are interspersed in a salt and pepper fashion (Ohki and Reid, 2007).

1.2 Dendritic integration

Information processing is carried out not only at the circuit level but also at single neuron level. As a computing device in micrometer scale, a neuron receives thousands of incoming inputs at their dendrites and integrate all the information to generate output in the form of action potentials. Action potentials are not generated inherently if the neurons are at rest because the membrane potential at rest (< - 70 mV) is lower than the action potential threshold (~ -50 mV). On the other hand, action potentials will be produced if the synaptically induced postsynaptic potentials (PSPs) could depolarize the membrane potential to the action potential threshold. The algorithm of PSPs summation has been investigated intensively *in vitro* regarding the properties of dendrites and spines (where most excitatory synapses reside). However, the summation algorithm is still largely incomplete for *in vivo* condition.

1.2.1 Passive and active properties of dendrites

The word dendrite comes from the Greek word déndron which means ‘tree’. Dendrites are those long processes that extend from the soma of neurons and branch like a tree. Different branching patterns endow neurons with distinct morphologies and are indicative of their functions. The morphology for an excitatory neuron in neocortex can be either stellate or pyramidal. Typically, the dendritic tree of pyramidal neurons has two distinct compartments, the basal dendrites, and the apical dendrites. The basal dendrites are distributed around the soma while the apical dendrites can be very long depending on the depth of the neuron. This highly polarized morphology implies the potential of differential afferents targeting the basal versus apical dendrites.

An early attempt to address the function of dendrites in dendritic integration was to think dendrites as passive cables. Therefore, the propagation and integration of PSPs inside the cable were determined by the electrical properties of the cable: membrane resistance, membrane capacitance, and intracellular resistance. By estimating these properties and optimizing the model, this theory could partially explain some linear and nonlinear operations in the dendrites (Koch et al., 1983; Rall, 1964).

In fact, dendrites are not membranous tubes but are equipped with several types of ion channels. Those ion channels are supposed to support the active properties of

dendrites and include voltage-gated sodium channels, voltage-gated calcium channels (VGCC), and voltage-gated potassium channels, and hyperpolarization-activated cation channels. Each type also has subtypes and distinct distribution pattern on the dendrites (Stuart and Spruston, 2015). Besides voltage-gated ion channels, there are also NMDA receptors on the dendrites of pyramidal neurons.

An interesting yet relatively new dendritic phenomenon that relies on the active properties of dendrites is the generation of dendritic spikes. Dendritic spike is the local voltage-dependent membrane potential event independent of the generation of the action potential at axon initial segment. The idea of a spike-like event on dendrites came up very early (Spencer and Kandel, 1961). The direct recording of a dendritic spike was not possible until the development of dendritic patch-clamp recording technique (Stuart et al., 1993). Dendritic spikes have been identified on the dendrites of various types of neurons *in vitro* and can be classified into three types: sodium (Stuart et al., 1997), calcium (Amitai et al., 1993; Schiller et al., 1997) and NMDA (Schiller et al., 2000) spikes. They are generated by activation of voltage-gated sodium channels, voltage-gated calcium channels, and NMDA receptors respectively. However, those studies on dendritic spikes were carried out on brain slices, raising the question whether dendritic spikes exist and function *in vivo*.

Recent works have confirmed the existence of dendritic spikes *in vivo* by patch-clamp recording (Gambino et al., 2014; Larkum and Zhu, 2002; Lavzin et al., 2012; Smith et al., 2013; Waters et al., 2003; Xu et al., 2012; Zhu and Connors, 1999) and two-photon calcium imaging (Grienberger et al., 2014; Murayama et al., 2009; Palmer et al., 2012, 2014; Sheffield and Dombeck, 2015; Xu et al., 2012). These studies included experiments performed with either anesthetized or awake animals, demonstrated that dendritic spikes play an important role in sensory information processing and sensory related behavioral tasks.

1.2.2 Dendritic spines

Dendritic spines are small membranous structures that protrude from the dendrites and can be found on many different types of neurons, for instance, pyramidal neurons in the neocortex (which will be the main focus of the following description). Dendritic spines have various morphologies depend on types of neurons or developmental

stages. The most common dendritic spine is the simple spine which is the site of more than 90% excitatory synapse in the brain. The typical simple spine is mushroom-shaped with a bulbous head and a thin neck. This peculiar morphology raised many hypotheses about its function. Among these, an intuitive one stated that dendritic spines increase the surface area of the dendrites which allows the formation of more synapses. However, this hypothesis is not supported by the fact that each spine usually contains a single synapse. Another reasonable hypothesis is that dendritic spines could serve as isolated biochemical and electrical compartments from dendritic shafts (Hering and Sheng, 2001; Shepherd, 1996; Yuste, 2013). As biochemical compartments, spines can partially isolate molecules between the spine head and the dendritic shaft (Colgan and Yasuda, 2014). One example is the confinement of Ca^{2+} inside a single spine (Yuste and Denk, 1995). As isolated electrical compartments, synaptically induced depolarization is larger in spines than that in dendritic shafts because of the high resistance of the spine neck (Yuste, 2013).

Dendritic spines are not merely membranous structures but are functional subcellular compartments. They contain several kinds of intracellular components, including smooth endoplasmic reticulum, polyribosomes, mitochondria, etc. On the membrane of dendritic spines, there exist AMPA receptors (AMPARs), NMDA receptors (NMDARs), voltage-gated calcium channel (VGCC) and so on (Fig. 3).

One of the most important biochemical signals in dendritic spines is intracellular Ca^{2+}. Ca^{2+} as a crucial second messenger in the spine head can activate various downstream calcium-binding proteins, including calmodulin, Ca^{2+}/calmodulin-dependent protein kinase II (CaMKII), small conductance Ca^{2+}-activated potassium channels, calcineurin, and calpain. These proteins will then regulate the functional and structural properties of spines.

The influx of Ca^{2+} into the spine head can be triggered by either synaptic activation or back-propagating action potential (bAP). In the case of synaptic activation, Ca^{2+} enters the spine through glutamate receptors. Glutaminergic inputs will first open AMPA receptors. Then, if the depolarization caused by the AMPA receptor opening is strong enough, NMDA receptors will also be activated. (AMPARs and NMDARs are nonselective cation channels with different permeability for Ca^{2+}. AMPARs without GluR2 subunit have higher Ca^{2+} permeability than other AMPARs and NMDARs are

particularly permeable for Ca^{2+}). In addition to glutamate receptors, additional Ca^{2+} influx is from VGCC and may be from internal Ca^{2+} stores such as mitochondria and endoplasmic reticulum. On the other hand, action potentials generated at the axon can backpropagate into the proximal dendrites and spines on those dendrites, causing a Ca^{2+} influx in dendrites and spines through VGCC (Markram et al., 1995). In certain cases, if synaptic inputs is paired with and just before bAPs, the pairing will induce a supralinear Ca^{2+} signal. This supralinearity is due to additional influx of Ca^{2+} through NMDARs and it happens only when depolarization caused by bAPs is strong enough to remove Mg^{2+} from NMDARs (Koester and Sakmann, 1998).

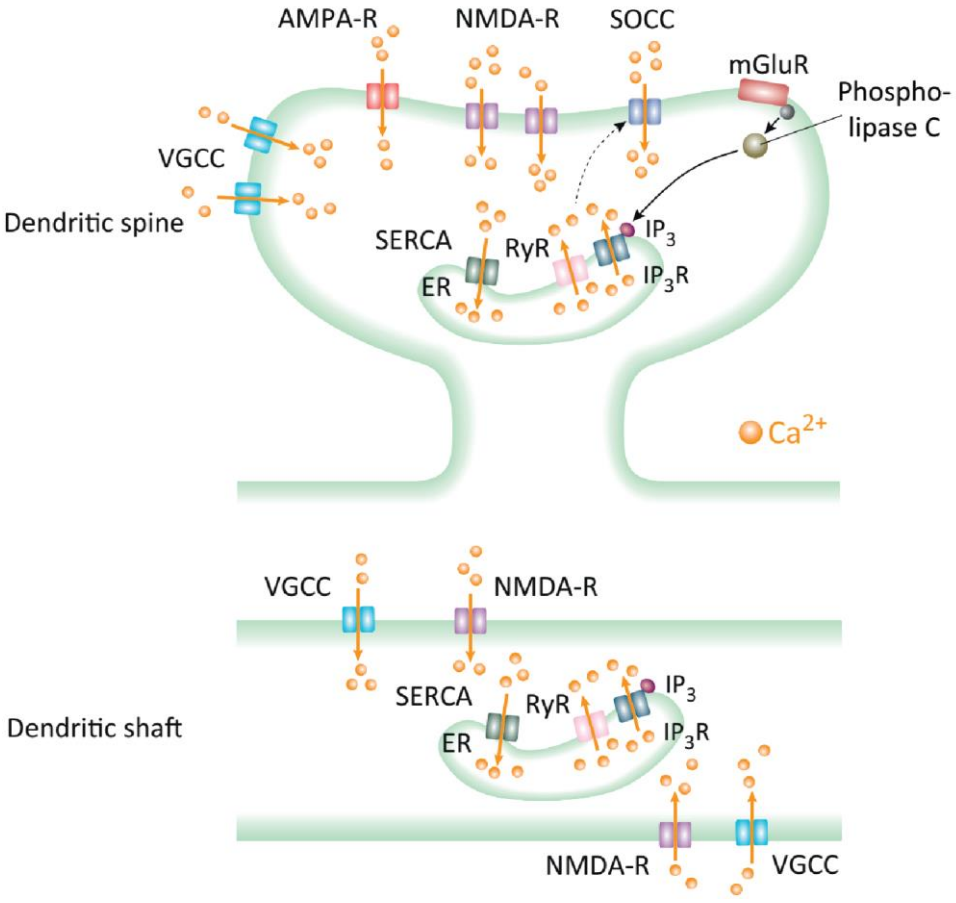

Fig. 3. Ca^{2+} sources in dendritic spine and dendritic shaft. Top, diagram of Ca^{2+} influx pathways in dendritic spine. Bottom, diagram of Ca^{2+} influx pathways in dendritic shaft. VGCC, voltage-gated Ca^{2+} channel. AMPA-R, AMPA receptor. NMDA-R, NMDA receptor. SOCC, store-operated Ca^{2+} channel. mGluR, metabotropic glutamate receptor. SERCA, sarco/endoplasmic reticulum Ca^{2+} ATPase. RyR, ryanodine receptor. ER, endoplasmic reticulum. IP_3, inositol trisphosphate. Diagram reproduced from (Grienberger et al., 2015).

The Ca^{2+} signal in dendritic spines not only is an essential second messenger to synaptic integration but also can be used as an indicator to study synaptic activity. Investigation of synaptic activity was performed extensively *in vitro* by staining the neuron with a Ca^{2+} indicator (Araya et al., 2006; Polsky et al., 2004; Tamás et al., 2002). Those studies established that coactivation of clustered spines could produce supralinear summation. However, those studies were performed using dissociated tissues and unphysiological stimulations which could not reflect dendritic integration in the living brain. New advancements in two-photon microscopy made it possible to record sensory stimulation evoked responses from anesthetized animals. Several pioneering experiments investigated sensory stimulation induced dendritic and spine responses (Chen et al., 2011; Jia et al., 2010; Varga et al., 2011). However, there was no evidence for synaptic clustering and supralinear summation in dendrites of layer 2/3 pyramidal neurons from the auditory, visual and somatosensory cortex. Recently, two studies using either lightly anesthetized mice or young ferrets reported clustering of spines favoring similar visual features in visual cortex (Iacaruso et al., 2017; Wilson et al., 2016). Despite several studies, there is still no definite conclusion as to the rules and algorithms of synaptic integration *in vivo*.

1.3 Aim of the study

There are certain distinct features that make L4 neurons in mouse V1 worth investigating. L4 neurons exhibit extremely high similarity in response properties (especially the degree of orientation selectivity) to that of other mammals without a functional cortical microstructure. As thalamorecipient neurons, L4 neurons have a nonclassical pyramidal morphology instead of a classical stellate morphology. Along with the recent finding that mouse LGN provides orientation selective inputs to multiple layers of V1, a critical question that needs to be answered is how L4 neurons in mouse V1 integrate LGN inputs to generate orientation selectivity. In this thesis, the following points regarding this question will be addressed:

1. Do L4 neurons in mouse V1 show robust and reliable response to drifting grating stimulation?
2. What kind of inputs do L4 neurons receive on the tuft dendrites? Are the inputs sparsely distributed or clustered?
3. How do tuft dendrites of L4 neurons integrate synaptic inputs? Are synaptic inputs integrated linearly or supralinearly?
4. What is the cellular mechanism of dendritic processing in tuft dendrites of L4 neurons?

2 Materials and Methods

2.1 Animals

All experimental procedures were performed in accordance with institutional animal welfare guidelines and were approved by the state government of Bavaria, Germany. Adult (~P60) C57Bl/6 mice of both sexes were used in most experiments. In some, Scnn1a-Tg2-Cre transgenic mice (both sexes) were used for sparse labeling of layer 4 pyramidal neurons with GCaMP6s. GCaMP6s virus was injected at around P35 and experiments were performed after P50. All mice were housed in the animal facility (12 hr light/dark cycle).

2.2 Drugs and solutions

Throughout the experiment, the recording chamber was perfused with warm (37 °C) artificial cerebrospinal fluid (ACSF) which contained: 125 mM NaCl, 26 mM $NaHCO_3$, 4.5 mM KCl, 2 mM $CaCl_2$, 1.25 mM NaH_2PO_4, 1 mM $MgCl_2$ and 20 mM glucose (pH 7.4 when bubbled with 95% O_2 and 5% CO_2). The staining solution used to label L4 neurons with Cal-590 AM was prepared as previously reported (Tischbirek et al., 2015). Briefly, 50 µg Cal-590 AM was first dissolved in 4 µl DMSO with 20% Pluronic-127 and then diluted in a HEPES-based ACSF (the final solution: 500 µM Cal-590 AM, 150 mM NaCl, 2.5 mM KCl, 10 mM HEPES and 20 µM Alexa 594). The staining solution was filtered by a 0.45 µm Millipore centrifuge filter. For cell-attached recording, ACSF containing 50 µM Alexa 488 was used. For whole-cell recording, intracellular solution contained: 135 mM K-gluconate, 4 mM KCl, 10 mM HEPES, 4 mM Mg-ATP, 0.3 mM Na_2-GTP, 10 mM Na-Phosphocreatine and 100 µM Oregon Green 488 BAPTA-1 hexapotassium salt (OGB1-6k). In some experiments, 2 mM MK-801 was added for blocking NMDA receptors intracellularly. For extracellular local drug application, ACSF contained 20 µM Alexa 594 and one of the following drugs was used: 100 µM D-(-)-2-Amino-5-phosphonopentanoic acid (APV), 100 µM 6-Cyano-7-nitroquinoxaline-2,3-dione (CNQX), 100 µM 4-(8-Methyl-9*H*-1,3-dioxolo[4,5-*h*][2,3]benzodiazepin-5-yl)-benzenamine dihydrochloride (GYKI 52466, GYKI), 10 µM tetrodotoxin (TTX) and 100 µM R(+)-Baclofen hydrochloride (baclofen).

2.3 Anesthesia

Anesthesia of the mouse was induced in an induction chamber with 2% (vol/vol) isoflurane (CP-Pharma, Burgdorf, Germany) in pure oxygen. After anesthesia induction, the mouse was transferred to the surgery table and supplied continuously with 1% isoflurane through a mask. Before all surgical procedures, a supplemental analgesic metamizole (200 mg/kg, s.c.) was injected. A local anesthetic (2% xylocaine, s.c.) was also injected at the site of surgery. During surgery, the body temperature of the mouse was monitored and maintained by a warm plate (38 °C). Both eyes were covered with ophthalmic ointment to prevent them from drying.

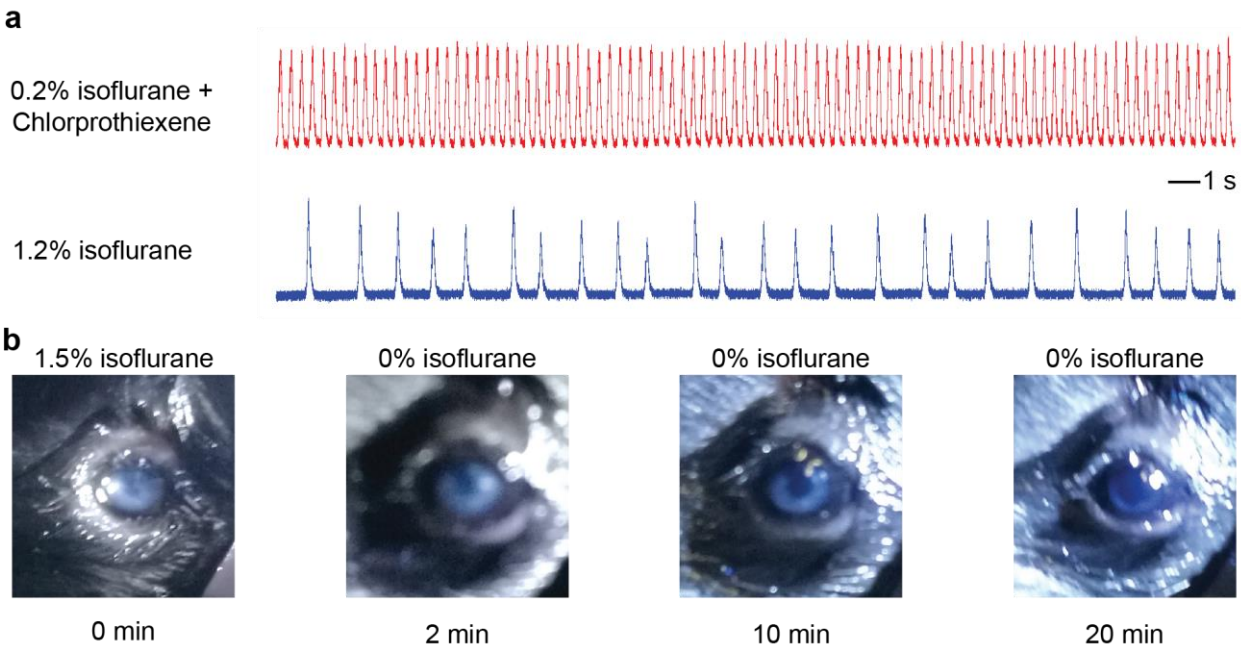

Fig. 4. Influence of isoflurane anesthesia on respiration and eye clarity. a, Top, respiration activity in light anesthesia (0.2% isoflurane + Chlorprothixene). Mouse breathing was fast (~ 180 BPM) and smooth under this condition. Bottom, respiration activity in deeper anesthesia (1.2% isoflurane alone). Mouse breathing was slow (~ 60 BPM) and irregular under this condition. **b,** Cataract induced by deep anesthesia. The eye of the mouse gradually became clear once isoflurane was removed.

Deep anesthesia with isoflurane has been shown to have profound effects on neuronal activity (Adelsberger et al., 2005; Raz et al., 2014; Villeneuve and Casanova, 2003). High concentration of isoflurane was also known to cause respiration difficulties and cataract (Fig. 4). These side effects made in vivo recording of neuron activity unstable especially activity induced by visual stimulation. In the present study, a light anesthesia

method was adopted to solve this problem (Niell and Stryker, 2008; Smith and Häusser, 2010). Before the start of recording, the mouse was injected with a sedative chlorprothixene (2.5 mg/kg, s.c.). After the sedation, the concentration of isoflurane can be decreased to 0.2%, and this concentration was maintained during recording. If the animal showed slight movement, the concentration of isoflurane was gradually increased until the movement stopped. The maximum concentration of isoflurane used for recording was 0.4%.

2.4 Surgery

The surgery was performed under a dissecting microscope. Around 5 min after injection of local anesthetic, the scalp above the visual cortex was carefully removed by fine scissors. The connective tissue between skin and skull was cleaned by gentle scraping of the skull surface with a No. 11 scalpel. The cleaned skull surface was allowed to dry for 5 min. The location of the mouse V1 (AP: 3.8 mm from bregma, ML: -2.5 mm from midline) was identified based on a mouse brain atlas and was marked on the skull. A thin layer of light-cure dental glue (OptiBond) was applied evenly on the skull, but the V1 area was avoided. After several seconds of drying, the glue was cured by blue light for 20s. A plastic recording chamber was then attached to the skull (Fig. 5). The recording chamber was made from a 35 mm diameter cell culture dish. A 4-mm diameter round opening was made close to the edge of the chamber for imaging access, the area surrounding the hole was abraded to fit the curvature of the skull. A thin layer of OptiBond was also applied to the edge of the hole on both sides and cured by blue light. For implantation of the chamber, a type of light-cured dental filling material (Tetric EvoFlow) was applied around the hole on the bottom side in a ring-shaped manner. The chamber was later put on the head of the mouse and pressed against the skull with V1 marker in the center of the hole. Tetric EvoFlow spread evenly in the space between skull and chamber. Blue light was immediately applied to cure Tetric EvoFlow for 20s. The chamber and the mouse were then fixed to a surgical frame made from acrylic. Under a dissection microscope, spaces and holes between the chamber and skull surface were also filled with Tetric EvoFlow and it was cured by blue light.

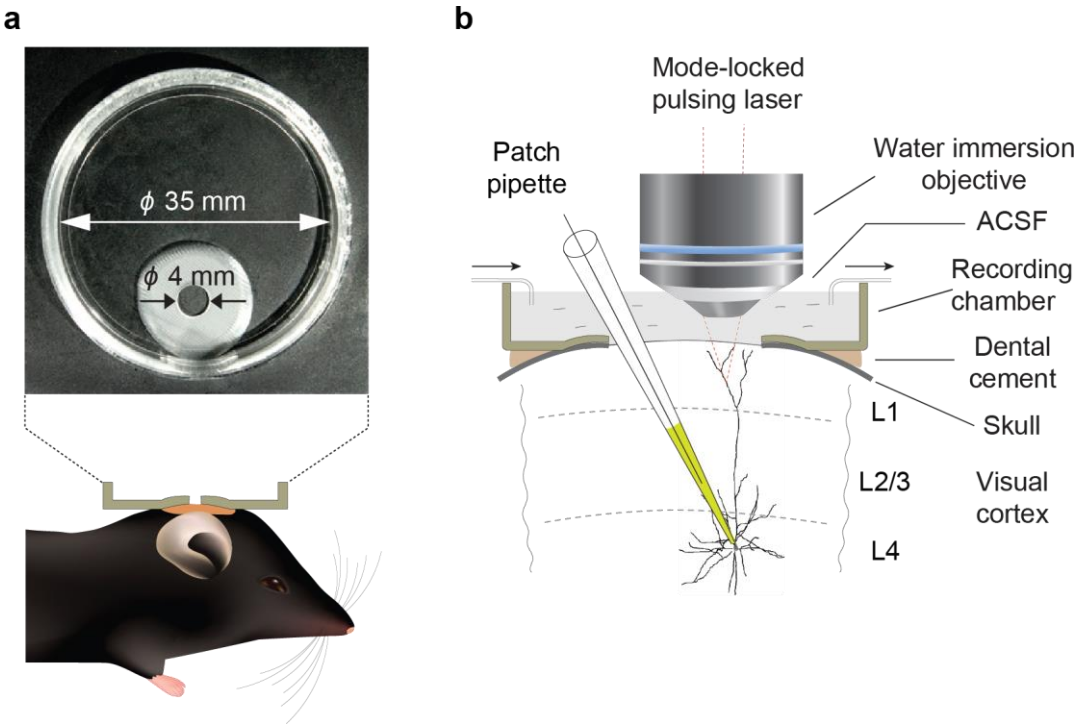

Fig. 5. Diagram of the experiment. a, Top, a custom-made recording chamber. Bottom, the way to fix the chamber to the head of the mouse. **b,** Scheme of simultaneous dendritic calcium imaging and cell-attached recording of an L4 neuron. Diagram reproduced from (Chen et al., 2012).

A square-shaped cranial window (1 mm x 1 mm) was made in the position of the V1 marker. The skull was first thinned at the edge of the square with a high-speed dental drill and a fine drill bit. Skull thinning is the most critical step in the making of craniotomy. The drill bit should not be pressed too hard against the skull, as strong vibration and pressure could break the underlying blood vessels. The drill bit should also not stay on the skull for too long, as the heat generated during thinning could damage the brain tissue. After thinning, a 30-gauge needle was used to cut the thinned edge of the square. Three sides of the square were cut by the needle, and ultra-fine forceps could then be inserted into the space between the brain tissue and the skull. The square-shaped skull piece was gently lifted and removed. Before removing the skull piece, the chamber was already filled with room temperature ACSF. Blood on the brain surface was cleaned by gentle puffing of solution when the skull piece was removed. Gentle puffing was intermittently applied whenever there was bleeding. Usually, the bleeding stopped within 5 min. In cases of heavy bleeding that could not be stopped in 10 minutes, the mouse was discarded according to the experimental protocol.

2.5 Virus injection

Mice were anesthetized as previously described and transferred to a stereotaxic instrument with continuous 1.5% isoflurane supply. The head of the mice was fixed on the stereotaxic instrument by clamping the front teeth with a teeth bar and inserting ear bars into the outer ear canals on both sides. Consequently, the head, once firmly fixed onto the instrument, should not be moved by gentle touching with forceps. The hair of the mice above the surgical area was trimmed by scissors. Exposed skin was disinfected with Povidone-iodine and ethanol. After injection of local anesthetic, an incision was made by cutting the skin from the middle of the two eyes to the middle of the two ears. The skin was retracted laterally to expose the skull. The site for inserting the injection micropipette was identified and marked on the skull based on a mouse brain atlas. A small hole was made at the marked location on the skull with a high-speed dental drill. The dura was pierced by a 30-gauge needle.

The micropipette for virus injection was prepared from a precision glass capillary using a vertical pipette puller. The micropipette was calibrated to inject a small volume of liquid in nanoliter range. The injection micropipette was held by a pipette holder mounted on the stereotaxic instrument. The blunt end of the pipette was connected to a syringe through a thin tube. A drop of virus solution was placed onto a small piece of parafilm and the tip of the micropipette was moved into the liquid drop using the manipulator of the stereotaxic arm. Virus solution was loaded into the micropipette by applying negative pressure with the syringe. Then, the micropipette was slowly moved to the targeted injection coordinate in the brain. The injection was achieved by applying positive pressure through the syringe. The speed of injection was controlled by monitoring the movement of the liquid level inside the micropipette and adjusting the pressure accordingly. Injection speed should be as slow as possible to reduce tissue damage (20 nl / min). After injection, the micropipette stayed inside the brain for another 5 min to allow diffusion of virus in the tissue before being retracted.

For sparse labeling of L4 neurons, Cre-dependent GCaMP6s virus was used (AAV1.Syn.flex.GCaMP6s.WPRE.SV40, 10^{13} genome copy per ml). The virus solution was diluted 5 times with PBS and 100 nl of the diluted virus was injected in layer 4 of V1 (AP: -4.0 mm from bregma, ML: -2.5 mm from midline, DV: -0.4 mm from brain

surface). The injection micropipette was advanced into the targeted depth in an oblique way to avoid damaging tuft dendrites of L4 neurons.

To label axonal boutons projecting from dLGN to V1, neurons in dLGN need to express GCaMP6s. Here we used the standard GCaMP6s virus to label LGN neurons. The virus (AAV1.Syn.GCaMP6s.WPRE.SV40, 10^{13} genome copy per ml) of 20 nl was injected into dLGN (AP: -2.3 mm from bregma, ML: 2.0 mm from midline, DV: -2.6 mm from brain surface). The injection pipette was advanced vertically to the targeted injection site.

After finishing all procedures, the scalp was closed with surgical suture and tissue glue (Vetbond). Metacam (1.5mg/kg, s.c.) was injected at the end and also for the following three days to reduce post-operational pain.

2.6 Two-photon microscope

Two-photon imaging was performed with a custom-built two-photon imaging system. The microscope was built based on a commercial upright microscope (Slicescope, Scientifica). A trinocular observation tube optimized for the infrared laser (U-TR30IR, Olympus) and a custom-built scanning unit was mounted on the microscope. The scanning unit was implemented with a 12-kHz resonant scanning mirror (Cambridge Technology) for fast scanning in the X direction and a standard galvanometric mirror for slow scanning in the Y direction. Fluorescence excitation light was provided by two laser sources. A mode-locked Ti:sapphire laser (Vision-S, Coherent) with 75 fs pulse width and 80 MHz repetition rate was used to deliver the laser at 920 nm wavelength. A second fiber laser (LightWire FF3000, EKSPLA) with a pulse width of 190 fs and a repetition up to 40 MHz was used to deliver the laser at 1064 nm wavelength. The output power of the 1st laser was controlled by a Pockels cell (Conoptics), and that of the 2nd was controlled by a half-wave plate (AHWP05M-950, Thorlabs) and a motorized precision rotation stage (PRM1/MZ8, Thorlabs). The two lasers were converged to the same light path by a polarizing beamsplitter cube (CM05-PBS203, Thorlabs). A long working distance water-immersion objective (40x, NA 0.8, Nikon) was used to allow simultaneous two-photon imaging and electrophysiological recording. In some experiments, multifocal plane imaging was performed, using a piezo objective scanner (P-725, PI) installed between objective and the microscope.

Emitted photons were detected by a hybrid photodetector (R7110U-40, Hamamatsu), amplified by an amplifier (DHPCA-100, Femto) and digitized by a high-speed digitizer (PXIe-5122, National Instruments). The controlling of the scanner and acquisition of data was achieved by an FPGA board (PXI-7851R, National Instruments). Just next to the microscope, a motorized XY stage was placed to hold the animal and electrode manipulators. XY position of the imaging area was controlled by the motorized stage during the experiment. The whole imaging system was controlled by a custom-made software using LabVIEW.

2.7 Ca^{2+} imaging of neurons and dendrites

L4 neurons were stained with a red-shifted calcium indicator Cal-590 in its acetoxymethyl ester form (Cal-590 AM) using the multi-cell bolus loading (MCBL) method (Stosiek et al., 2003; Tischbirek et al., 2015). The dye loading pipette was prepared by pulling a 2-mm glass capillary with a vertical pipette puller. The shape of the pipette was similar to those used for electrophysiological recording but with longer taper and lower resistance (1 MΩ). The pipette was filled with staining solution and inserted into the brain under the guidance of two-photon imaging. Once the tip of the pipette reached layer 4 (between -350 μm and -450 μm from pia), the staining solution was injected by applying positive pressure through a syringe. The area of staining could be estimated by observing the diffusion of Alexa 594 in the tissue. The brain area above the site of staining should be free of big blood vessels. Otherwise, a new staining site had to be found. After injection, the pipette was retracted. A good staining was usually achieved 1h after dye injection (Stosiek et al., 2003).

To record calcium signals from L4 neurons labeled with Cal-590 AM, the 1064 nm laser was used. The laser power under the objective ranged from 60 mW to 100 mW. Images were recorded at 40 Hz frame rate. The imaging area covered around 100 μm by 100 μm and the imaging depth was restricted to layer 4.

For dendritic and spine imaging, neurons were labeled with either GCaMP6s or OGB1-6k. The 920 nm laser was used to excite GCaMP6s and OGB1-6k. The laser power under the objective for dendritic and spine imaging was lower than 20 mW. Images for dendritic and spine signal were recorded at 40 Hz, 80 Hz or 100 Hz frame rate.

2.8 Single-cell electroporation and electrophysiological recording

Single-cell electroporation has become a useful technique for studying morphology and function of single neurons since its development in vitro (Nevian and Helmchen, 2007) and in vivo (Chen et al., 2012; Judkewitz et al., 2009; Kitamura et al., 2008). Molecules like fluorescence dyes, ion indicators, and even plasmids can be introduced into single cells by electroporation. Traditionally, single-cell electroporation used to be performed on randomly chosen cells. The response of the cell could not be predicted until doing electrophysiological recordings or calcium imaging. Therefore, it is not efficient to study the function of cells with certain behavior using this method. Electroporation of plasmids into cells with certain behavior was recently demonstrated (Wertz et al., 2015). However, this approach could only be used to study morphology and connectivity of neurons at the moment. To study dendritic properties of single neurons, we combined single-cell electroporation of a green calcium indicator with population imaging using a red calcium indicator. A large population of neurons were firstly stained with a red-shifted calcium indicator Cal-590 AM as previously described. The target neurons were identified by their response of interest (in our study, they were a subset of neurons showing strong responses to visual stimulation) and electroporated those neurons with a green calcium indicator OGB1-6k. Once a target neuron was identified, single-cell electroporation was performed as described previously (Chen et al., 2012; Hill et al., 2013; Jia et al., 2014). Electroporation pipettes were made with a vertical pipette puller, showing a resistance of 6 - 7 MΩ. The pipette was loaded with the intracellular solution containing 1 mM OGB1-6k. Coordinates of the target neuron in the brain were recorded and were used to estimate the coordinate for pipette insertion based on the angle of the pipette. The pipette was inserted into the brain at this estimated coordinate and was navigated in the brain using ‘shadow-patching’ method (Kitamura et al., 2008) to avoid neurons and blood vessels before reaching the target. The wavelength of the excitation laser was switched intermittently between 920 nm and 1064 nm to confirm the pipette was on the right route to the target. When the pipette was close to reaching the target neuron, the speed of the pipette was lowered to avoid damaging the surrounding tissue. The tip of the pipette was advanced to the center of the target neuron in both XY direction and Z direction. Optionally, gentle negative pressure could be applied to enhance the contact between the neuron and the pipette. The calcium indicator was injected by a short electrical

pulse. The electrical pulse had an amplitude of -200 nA and a duration of 30 ms and was generated by a modified intracellular amplifier (ELC-03M, NPI). Usually, a single pulse was sufficient to stain the neuron, if the first pulse failed in staining, a second pulse or more pulses were applied until the neuron was adequately filled. After electroporation, the pipette was retracted immediately. Sufficient filling of an L4 neuron with OGB1-6k was reached at least 45 min after electroporation.

Cell-attached recording of the electroporated neuron was performed similarly to what is for single-cell electroporation. For cell-attached recording, the recording pipette was loaded with ACSF containing Alexa 488. When the pipette was in contact with the neuron, relatively large negative pressure was applied to obtain a seal resistance of 40 – 60 MΩ. Electrophysiological data was acquired by a patch-clamp amplifier (EPC10, HEKA). The recording was made either in current clamp-mode or in voltage-clamp mode.

Also for whole-cell recording, the procedure resembled that for electroporation and cell-attached recording. The pipette used in whole-cell recording had a smaller resistance (4 - 5 MΩ) and was loaded with the intracellular solution containing 100 μM OGB1-6k. When the pipette was navigating in the brain, constant positive pressure (~ 20 mbar) had to be given to keep the tip clean. Just before touching the neuron with the pipette, relatively large positive pressure (~ 40 mbar) was applied to clean the surface of the neuron. The positive pressure was maintained when the pipette was in contact with the neuronal membrane and was not removed until the appearance of a small bright dimple on the surface of the neuron. Strong negative pressure (-70 mbar) was immediately applied to obtain a seal resistance in GΩ range. When the GΩ seal became stable, the sealed membrane was ruptured by gentle and brief negative pressure. The offset voltage and pipette capacitance were compensated during this process. The recording was acquired by an EPC10 amplifier in current-clamp mode. Whole-cell recording could be performed with or without electroporation on target neurons depend on the purpose. The time needed to stain a neuron through whole-cell recording was similar to single-cell electroporation.

2.9 Visual stimulation

A 7-inch LCD monitor (pixel resolution: 1280 x 800; refresh rate: 60 Hz) was used for visual stimulation. The brightness of the monitor was adjusted and calibrated by a photometer (gamma correction). As a result of calibration, the luminance for white screen, black screen and gray screen is 70 cd/m^2, 0 cd/m^2 and 35 cd/m^2 respectively. The monitor was placed 10 cm away from the contralateral eye of the mouse, which covered 76° in azimuth and 46° in elevation. A black cone made from paper was fixed between the monitor and the eye of the mouse to prevent screen light going into the light path of the microscope.

Visual stimulation was created by a custom-written MATLAB code using PsychToolbox (Brainard, 1997; Pelli, 1997). Visual stimulation consists of full-field square wave or sine wave drifting gratings of 8 directions (45° step) at 100% contrast, 0.04 cpd (cycle per degree) spatial frequency and 2 Hz and temporal frequency. Drifting grating of each direction was presented for 1 s with 2 s gray screen after stimulation. For each trial of visual stimulation, four seconds of gray screen was presented before and after a set of 8 directions stimulation to collect baseline activity. Calcium imaging and electrophysiological recording were synchronized with the visual stimulation by trigger TTL signals.

2.10 Pharmacology

Local drug application to neurons or dendrites was performed by a glass pipette similar to the one for bolus loading. The application was controlled by a syringe. The area of application was monitored by diffusion of Alexa 594.

2.11 Data analysis and statistics

All imaging and electrophysiology data were analyzed off-line using MATLAB. For imaging data with strong tissue movement, image stacks were corrected with a correlation based image registration algorithm before subsequent analysis (Guizar-Sicairos et al., 2008). To extract calcium signal, acquired image stacks were imported into MATLAB and mean projection images were generated by averaging all frames. Regions of interest (ROIs) were drawn manually on neuronal somata, dendrites or spines. Raw fluorescence signals (F) were extracted from each ROI. Baseline

fluorescence (F_0) was defined as the mean of fluorescence signals in two seconds before visual stimulation. Normalized fluorescence change was calculated by $\Delta F/F=(F-F_0)/F_0$.

Visual responsiveness was determined by comparing the activity across baseline period and drifting grating periods with one-way ANOVA test (Ohki et al., 2005). If the p-value was smaller than 0.05 and the maximum response in drifting grating periods was over 5 times standard deviation (SD) of baseline activity, the neuron, the dendrite, the spine or the bouton was considered visually responsive. Orientation selectivity was quantified by a circular variance-based method (Ringach et al., 2002; Swindale, 1998) and was calculated by the following equation:

$$r = \frac{\sum R(\theta_k) e^{i2\theta_k}}{\sum R(\theta_k)}$$

where r is the resultant, and $R(\theta_k)$ is the response to direction θ_k. The absolute amplitude of the resultant will give global orientation selective index (gOSI). The half amplitude of the complex phase of the resultant will give the preferred orientation. A neuron was orientation selective if its gOSI was larger than 0.33 (Kondo and Ohki, 2015). Direction selectivity index (DSI) was calculated by:

$$DSI = \frac{R_{pref} - R_{oppo}}{R_{pref} + R_{oppo}}$$

where R_{pref} is the response to preferred direction, and R_{oppo} is the response the opposite direction. A neuron was considered direction selective if its DSI was larger than 0.5 (Sun et al., 2015).

A z-stack of the recorded neuron was acquired at the end of each experiment, with 0.5 μm or 1 μm spacing in z-axis. Z-stack files were imported into ImageJ (Fiji) and dendrites were traced manually with Simple Neurite Tracer plugin.

All data were expressed as mean ± standard error of the mean (sem) unless otherwise stated. Statistical tests were performed using either MATLAB or Excel. F-test was used to determine equality of variances. Statistical test used in each data was stated in the figure legend.

3 Results

3.1 Orientation selectivity of L4 neurons in mouse V1

Response properties of L4 neurons in mouse V1 has been investigated by several researchers with either electrophysiological recording (Niell and Stryker, 2008) or two-photon calcium imaging (Kondo and Ohki, 2015; Sun et al., 2015). These studies showed a substantial amount of orientation and direction selective neurons in layer 4. However, these studies only investigated the tuning strength of L4 neurons, but not the response strength.

In the first part of our study, we characterized response properties of L4 neurons in mouse V1 with an optimized two-photon calcium imaging of neuronal populations for deep cortical layers. It was achieved by staining L4 neurons with a new red-shifted calcium indicator Cal-590 AM and in vivo two-photon calcium imaging with a long wavelength two-photon laser (1064 nm). The application of staining solution was controlled by monitoring the diffusion of Alexa 594 in the tissue. The staining area should be restricted to layer 4 as the staining of superficial layers will compromise the quality of final images. If the staining is successful, a clear image with donut-shaped neuronal somata will be seen (Fig. 6a). On the contrary, unsuccessful staining will give a fuzzy image with undiscernible neuronal somata.

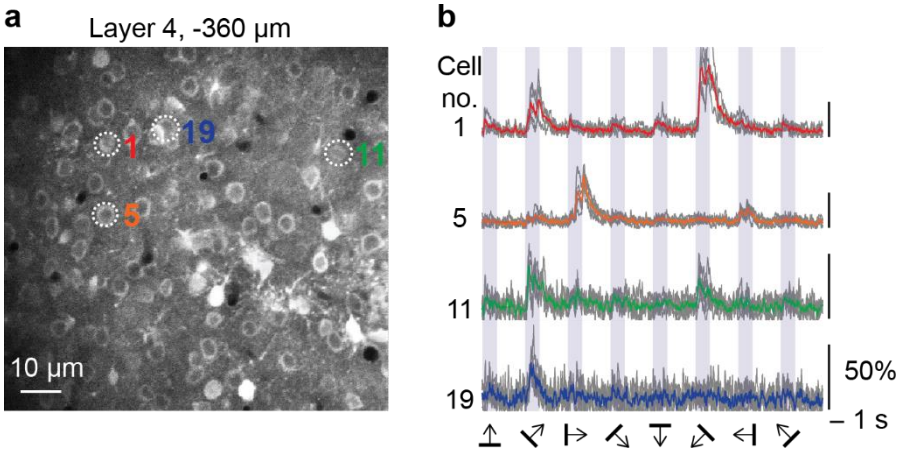

Fig. 6. In vivo two-photon calcium imaging in layer 4 of mouse V1. a, Two-photon image of L4 neurons stained with Cal-590 AM. The image was taken at the depth 360 µm below pia. **b,** Ca^{2+} transients evoked by visual stimulation from neurons indicated in **a**. Superimposed trials (gray, n = 5 trials) and average (colored) were shown. Shaded periods indicate visual stimulation with drifting gratings. Arrows at the bottom indicate the directions of drifting gratings.

To record visually evoked neuronal response, visual stimulation of drifting gratings was presented to the right eye of the animal, and real-time two-photon images were acquired simultaneously. Acquired image stacks were later imported into MATLAB, and fluorescence signals were extracted from neuronal somata. Normalized fluorescence signals (ΔF/F) were calculated and used for all the analysis.

Typical responses of L4 neurons to drifting grating stimulation were shown in Fig. 6b. Shaded bars indicated 1s of visual stimulation with drifting gratings. Arrows at each gray bar were directions of drifting gratings. Neurons were considered visually responsive if they showed large Ca^{2+} transients (see methods for criteria) to at least one of 8 directions of drifting grating stimulation. A neuron could be classified as orientation selective (OS) or direction selective (DS) based on its response pattern. Orientation selective neurons had similar Ca^{2+} transients to two different directions which were 180° apart (Cell 1 and 11 in Fig. 6b). Direction selective neurons responded with large Ca^{2+} transients to one direction and with no or much smaller Ca^{2+} transients to the opposite direction (Cell 5 and 9 in Fig. 6b). We quantified the tuning properties of all recorded L4 neurons from 9 mice and calculated their global orientation selective index (gOSI) and direction selective index (DSI) (see methods). Under our experimental condition, the median gOSI and the median DSI for the recorded neuron population were 0.22 (Fig. 7a) and 0.31 respectively (Fig. 7b).

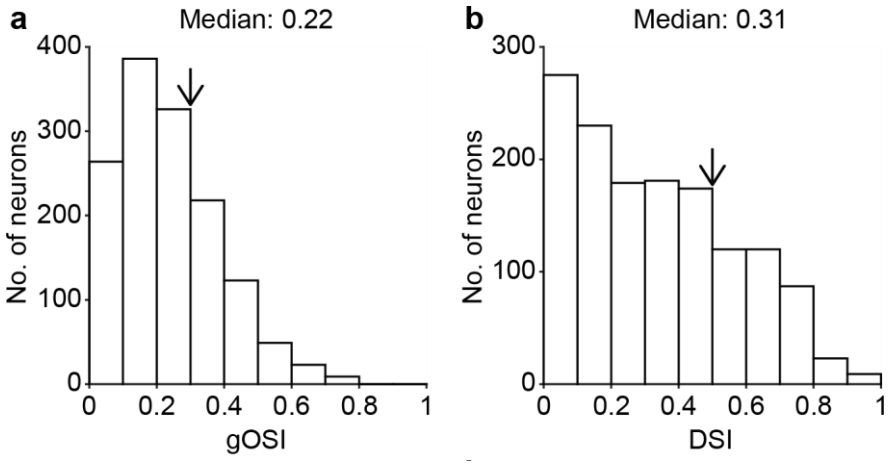

Fig. 7. Orientation and direction selectivity of L4 neurons in mouse V1. a, Distribution of gOSI in L4 neurons (n = 1398 neurons). **b,** Similar to **a**, for DSI. Arrows in **a** and **b** indicate the threshold for OS neurons and DS neurons.

3.2 Super responsive neurons in layer 4

An interesting observation from previous experiments was the huge difference in amplitudes of neuronal responses to visual stimulation (Fig. 6b). Then to what extent did neuronal visual responses differ from one another? In Fig. 6a, there were 80 neurons in the field of view, 38 of them were visually responsive based on the criteria. To compare the strength of responses, the amplitudes of response from all responsive neurons to preferred directions were measured and sorted. Plotting sorted amplitudes versus cell number revealed a surprisingly non-uniform distribution of responses strength (Fig. 8). Three neurons responded with very large amplitudes while the rest were with much smaller amplitudes.

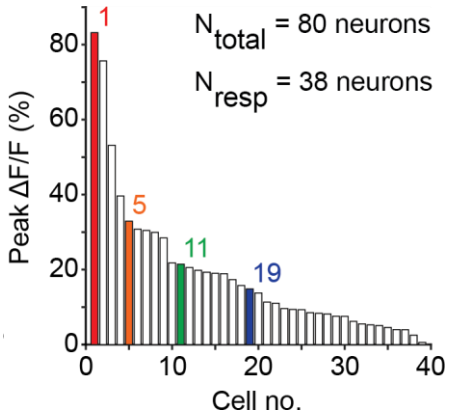

Fig. 8. Distribution of peak ΔF/F of L4 neurons in Fig. 6a. Each bar represented a single neuron. Neurons were sorted based on their response amplitudes to preferred directions. Colored bars corresponded to the four neurons in Fig. 6.

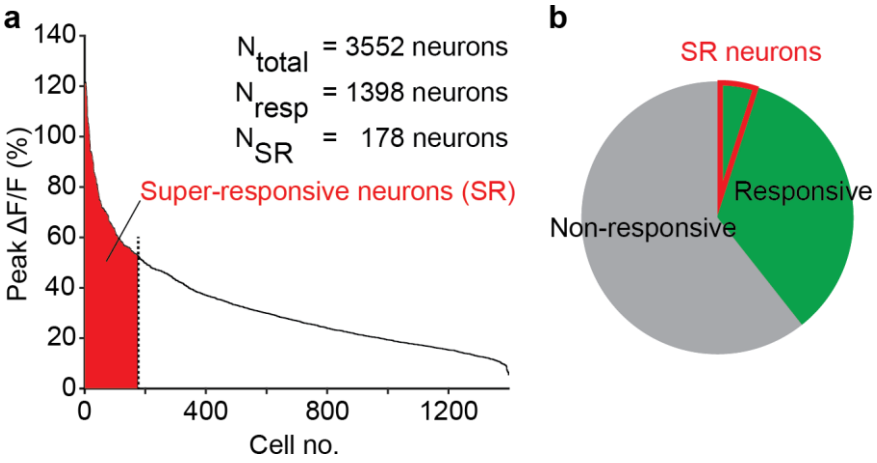

Fig. 9. Super responsive neurons in layer 4. a, Distribution of peak ΔF/F of all L4 neurons. **b,** Pie chart showing the proportion of different groups of L4 neurons.

Then we looked at the response strength of L4 neurons from a larger population. We pooled and extracted visually evoked responses of 3552 L4 neurons from 9 mice and identified 1398 responsive neurons (which is about 40% of the whole population). Plotting the amplitudes of all responsive neurons revealed a similar distribution as in Fig. 8. The distribution of amplitudes showed a two-phase decay and could be fitted perfectly to a double exponential function (Fig. 9a).

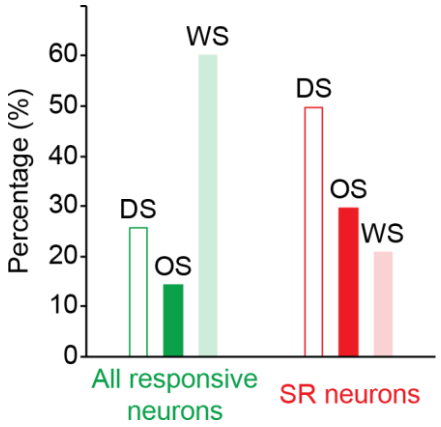

Fig. 10. Ratio of tuned neurons in different populations. DS, direction selective. OS, orientation selective. WS, weakly selective.

In particular, we found the top 5% of all recorded neurons showing much larger (more than 50% ΔF/F) and reliable responses. These neurons were named super responsive (SR) neurons (Fig. 9a, b). To analyze the tuning properties of SR neurons, we defined neurons with more than 0.5 DSI as DS neurons and neurons with less than 0.5 DSI but with more than 0.33 gOSI as OS neurons. The rest were weakly selective (WS) neurons. With this standard, we found that in all responsive neurons population, there were a small portion of DS neurons (26%) and OS neurons (14%); the majority of the population were WS neurons (60%). However, in the SR neurons population, the percentage of DS neurons increased to 50%, and the percentage of OS neurons increased to 29%. The WS neurons became the minority (21%) (Fig. 10). This result showed that in the entire neuronal population there were only 40% of the neurons responding to certain visual features with high specificity while in the SR neurons population the number reached 79%. Clearly, SR neurons were not only strong in response strength but were also high in response specificity.

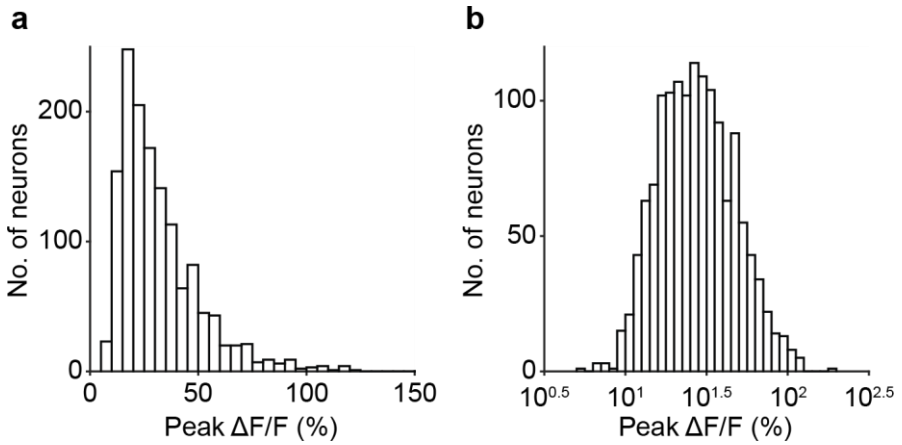

Fig. 10. Lognormal distribution of response strength of L4 neurons. a, Histogram of response strength in the standard scale. **b,** Histogram of response strength in the log scale.

To further appreciate the distribution of response strength of L4 neurons, we made a histogram of the response amplitudes. The histogram showed that the response amplitudes of all responsive neurons followed a lognormal distribution (Fig. 10a). Most neurons fell in the range of low response amplitude while a small portion was in large response range. The lognormal distribution was further supported by the evidence that if x-axis is in log scale, the data will have a perfect normal distribution (Fig. 10b).

The idea that biological parameters have a lognormal distribution is not new as this was already shown to be true for synaptic strength, neuronal firing rate and so on (Buzsáki and Mizuseki, 2014). The skewed distribution of neuronal activity may suggest a basic principle of information processing in the brain that a minority of strong responsive neurons can provide a substantial portion of brain activity and process most of the tasks. Therefore, it will be essential to investigate the properties of the small set of strong responsive neurons.

Intracellular Ca^{2+} is highly correlated with neuronal activity (number of action potentials) as each action potential will cause a certain amount of Ca^{2+} influx into the neuron. Measuring the change of intracellular Ca^{2+} is an indirect way to quantify neuronal activity (Mao et al., 2001). However, calcium imaging data can only give a relative response strength of a neuron. It may reflect the activity precisely if a neuron is relatively silent. If a neuron is very active, the change of intracellular Ca^{2+} will not truly reflect its level of activity.

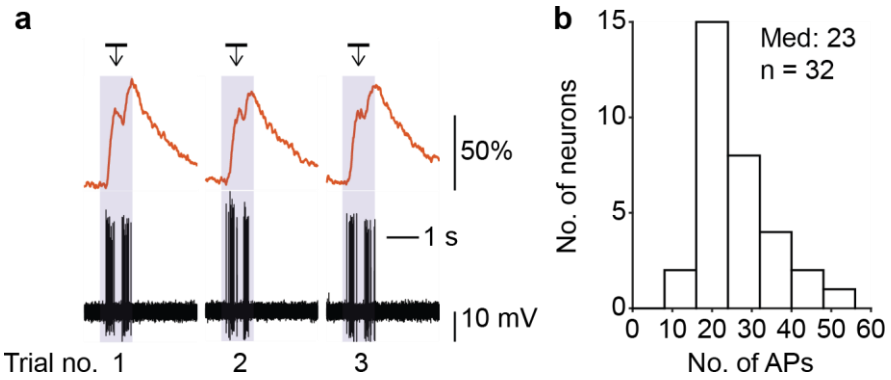

Fig. 11. Electrophysiological recordings from SR neurons. a, Simultaneous calcium imaging and cell-attached recording of an SR neuron**.** Red traces were calcium signals and black traces were electrophysiological recordings. Arrows denote the preferred direction of the neuron. **b,** Distribution of number of APs to the preferred direction.

To better quantify the response strength of SR neurons, electrophysiological recording of those neurons was needed. We then performed cell-attached recording on identified SR neurons in layer 4. Fig 11a showed a representative experiment in which in three consecutive trials the neuron responded to the visual stimulation reliably with high-frequency trains of action potentials. The histogram in Fig. 11b summarized the results from 32 recorded SR neurons and revealed that the median number of evoked APs was 23 when presenting the preferred direction of drifting grating stimulation.

3.3 Tuned dendritic tuft calcium signals in SR neurons

In the second part of our study, we explored the dendritic properties of SR neurons. To do this, we used a two-step approach. Firstly, SR neurons were identified by population calcium imaging as previously described. Then identified SR neurons were injected with the green calcium indicator OGB1-6K through a patch pipette. This could be done by either single-cell electroporation or whole-cell recording as described in the methods. By staining single cells with a calcium indicator with a different excitation wavelength, we can observe the calcium response of dendrites and spines from a functionally defined neuron without the contamination of background fluorescence.

Typically, neurons in layer 4 of mouse primary visual cortex usually had pyramidal morphologies and therefore got the name star pyramidal neuron. An example of such neuron was shown in Fig. 12a. The morphological inspection of such neurons demonstrated that most basal dendrites stayed in layer 4 while the apical dendrites reached the pial surface and formed small tufts with two secondary dendrites. The tufts eventually branched into a 3-4 thin distal dendrites (Fig. 12a).

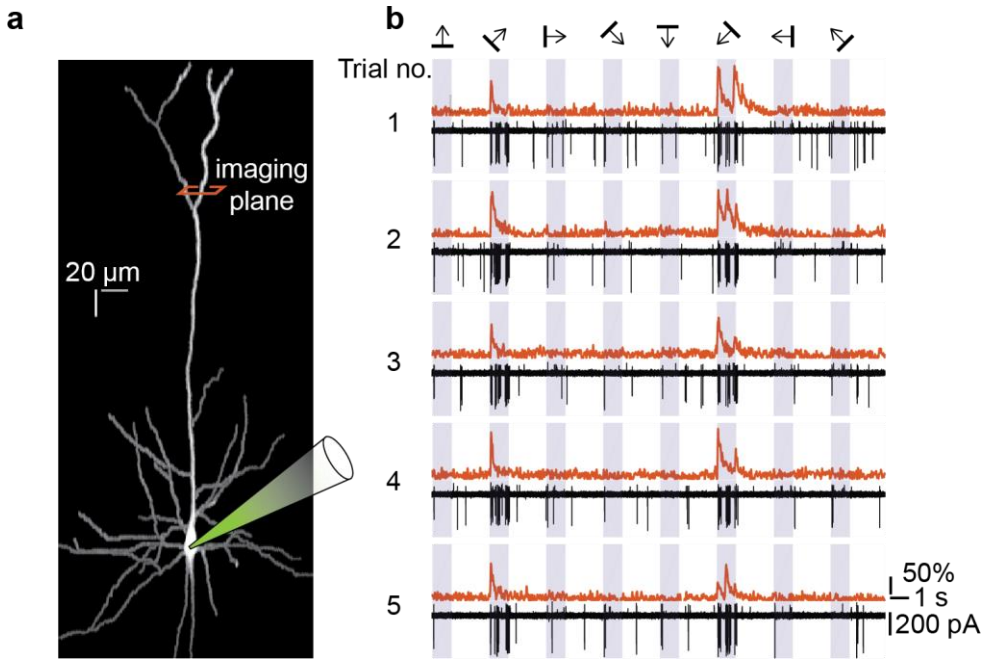

Fig. 12. Simultaneous dendritic calcium imaging and cell-attached recording of a single L4 neuron in vivo. a, Reconstructed morphology of a recorded L4 SR neuron. **b,** Example traces of simultaneous cell-attached recording and dendritic calcium imaging on tuft dendrites. Red traces were calcium signals and black traces cell-attached recordings.

Once a targeted SR neuron was sufficiently stained with OGB1-6k, we performed simultaneous cell-attached recording and dendritic calcium imaging on tuft dendrites. An example recording was shown in Fig. 12b. The neuron was firstly targeted with a micropipette to establish cell-attached recording. Then the imaging plane was focused on tuft dendrites of the neuron. Dendritic tuft calcium imaging was carried out between 0-100 µm below pia.

From the cell-attached recording in Fig. 12b, we could see that this neuron was highly responsive and highly tuned to two different directions of drifting gratings. These two directions were opposite to each other, but the gratings were orientated at the same angle. This neuron was thus orientation selective. It fired APs reliably from trial to trial and at a higher frequency (28 Hz) during the presentation of drifting grating in the preferred direction (Fig. 12b and Fig. 13b, c).

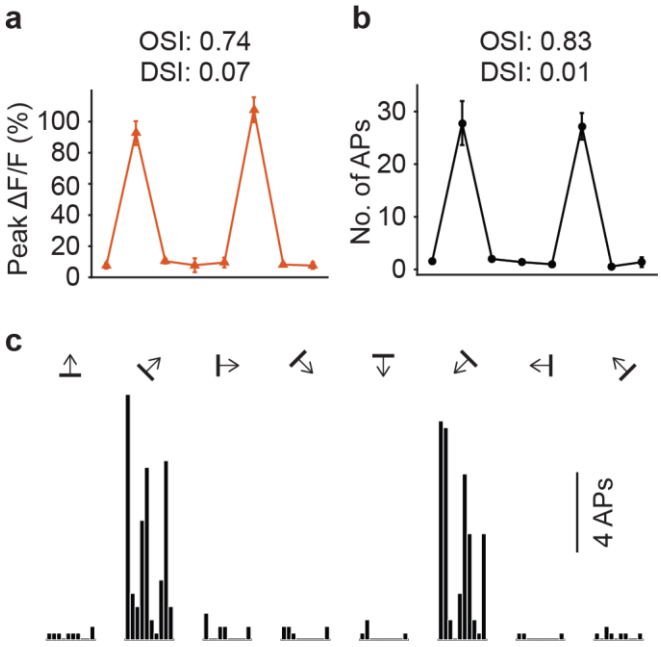

Fig. 13. Tuning properties of tuft calcium signals and somatic APs for the neuron shown in Fig. 12. a, Tuning curve of calcium signals on tuft dendrites. **b,** Tuning curve of somatic APs. **c,** Peristimulus time histograms (PSTHs) of AP response to different directions.

Apart from the highly tuned somatic response, tuned Ca^{2+} transients to the same orientation were also observed on the tuft dendrites (Fig. 12b and Fig. 13a). The observation of this distinct Ca^{2+} transients on the tuft dendrites of L4 neurons was unexpected. Dendritic calcium events are usually generated through back propagation

of action potentials. Those bAPs induced dendritic calcium events will attenuate along the dendrites with the increase of distance to soma. However, these Ca^{2+} transients we observed on the tuft dendrites are fast in rising time and large in amplitudes. Such large amplitudes could not be a result of attenuation of bAPs induced Ca^{2+} transients. It was also observed that single AP or several APs could not produce any Ca^{2+} transients on the tuft dendrites (Fig. 12b).

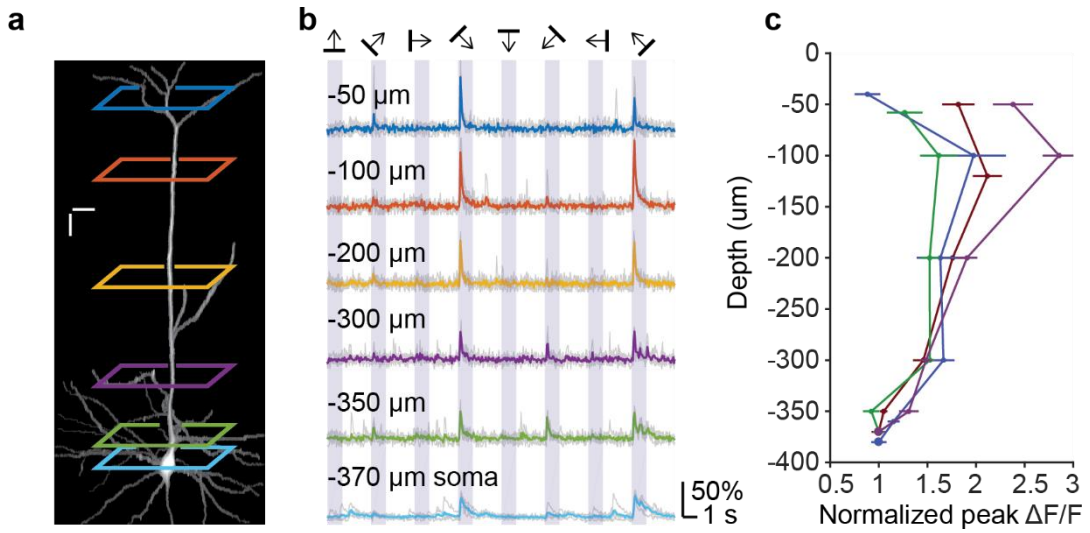

Fig. 14. Larger calcium responses on upper apical dendrites. a, Side projection of a recorded L4 neuron. Colored marks indicate imaging depth shown in **b**. **b,** Dendritic calcium recordings at different depths of the same neuron in **a**. Traces are single trials (gray) and their average (color). **c,** Response amplitudes at various depths of four L4 neurons.

We then recorded calcium signals from different depths of apical dendrites and found orientation selective Ca^{2+} transients across the whole apical dendrites (Fig. 14a). The amplitudes of those calcium transients were not even. Largest amplitude appeared on the upper part of apical dendrites (around -100 µm) while on lower apical dendrites only small amplitude Ca^{2+} transients can be found (Fig. 14b). This is not an accidental observation but was recorded from many neurons. The representative responses across different depths of apical dendrites from 4 neurons were shown in Fig. 14c. This observation suggested that the large amplitude Ca^{2+} transients were local calcium events restricting to the upper part of apical dendrites.

In Fig. 12 and Fig 13, the tuned Ca^{2+} transients had a similar preferred orientation to that of somatic responses. We found this match of preferred orientation between large

amplitude Ca^{2+} transients on tuft dendrites and somatic responses in all recorded SR neurons (Fig. 15).

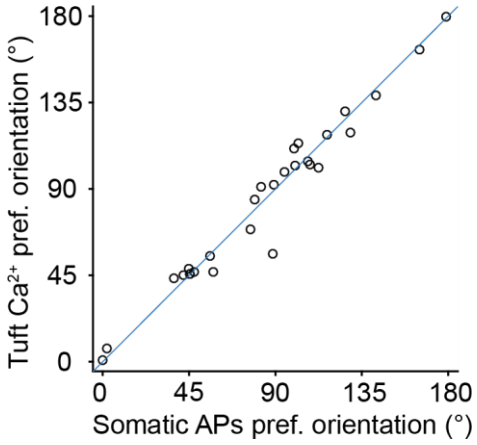

Fig. 15. Correlation of preferred orientation between tuft Ca^{2+} transients and somatic APs. Each circle represents a single neuron. (n = 27 neurons, r = 0.98, p < 0.001, Spearman's rank test)

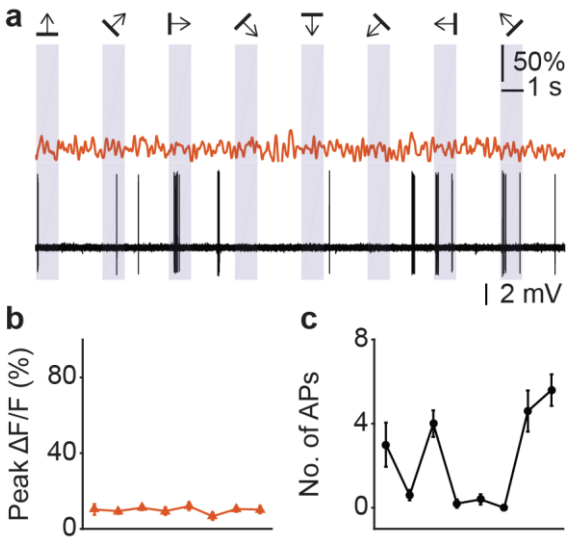

Fig. 16. Absence of dendritic calcium response on WS neurons. a, Simultaneous dendritic calcium imaging (red) and cell-attached recording (black) of an L4 WS neuron. **b,** Tuning curve of calcium signals on tuft dendrites. **c,** Tuning curve of somatic APs.

We also performed targeted recordings from WS neurons. Fig. 16 showed an example of this kind. The neuron was orientation selective but with a weak response (Fig. 16a). The mean firing rate was smaller than 10 Hz for the preferred direction of drifting grating stimulation (Fig. 16c). On the tuft dendrites, no large amplitude Ca^{2+} transient was observed (Fig. 16b). This potentially suggested that large amplitude Ca^{2+}

transients on the tuft dendrites were only associated with strong somatic firing and might be an indicator for SR neurons.

3.4 Dendritic calcium spikes are local

We next try to determine whether these dendritic calcium events are local. The best evidence of local dendritic spikes was that obtained by multiple dendritic recording in vitro. These studies illustrated the difference in spike waveforms at different dendritic locations. Such evidence was not provided when researchers tried to demonstrate the existence of dendritic spikes in vivo because of technical difficulty. We have recorded calcium events from different locations of an apical dendrite. The result showed an inequality of amplitudes across the whole apical dendrites with the largest amplitude on the upper part (Fig. 14). This gave us a clue that there might be local dendritic calcium spikes. However, those Ca^{2+} transients were not simultaneously recorded at multiple depths but were acquired sequentially at different depths.

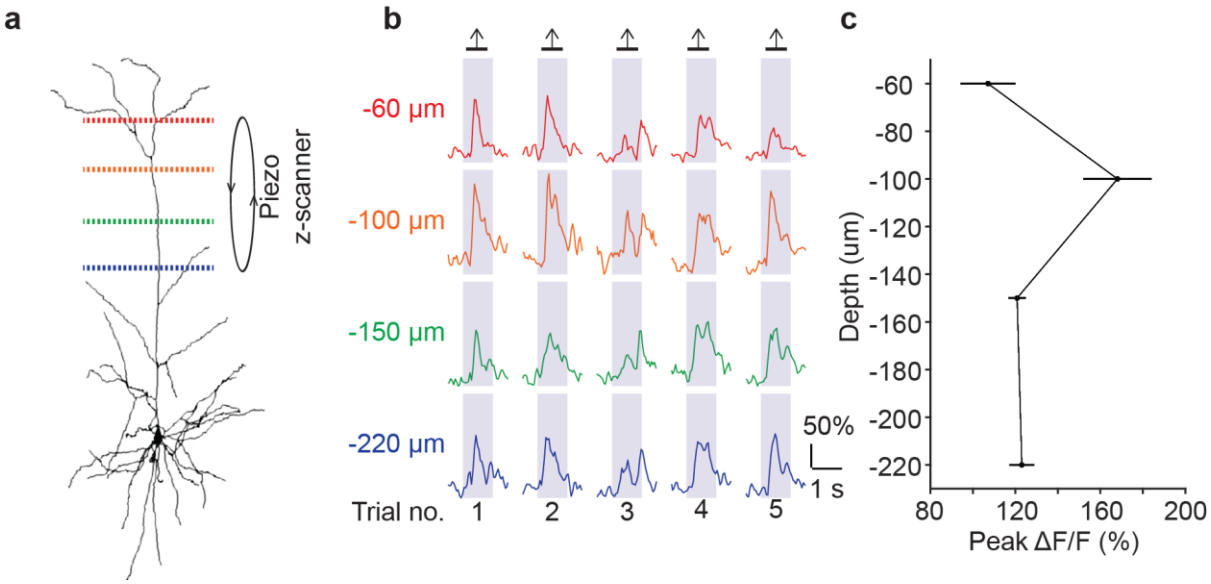

Fig. 17. Simultaneous imaging of apical dendrites at four depths from an L4 neuron. a, Reconstructed morphology of the recorded neuron. Dotted lines indicate recording depths shown in **b**. Ellipse with arrows illustrates the trajectory of objective driven by piezo z-scanner. **b,** Single trials of recordings from different depths. **c,** Maximum amplitudes of responses from different depths.

To acquire simultaneous recordings from several dendritic locations in vivo, two-photon calcium imaging in 3d volume is a good candidate. 3d two-photon calcium imaging has already been shown to be feasible by different researchers. Various methods utilizing acousto-optical deflector (AOD), piezo-driven objective and electrically tunable lens were being tested for neuronal population imaging. 3d two-

photon calcium imaging of neuronal dendrites was not possible until recently by using AOD. We used piezo-driven objective to achieve simultaneous dendritic calcium imaging from different depths as it was the easiest way and required minimal modification of the microscope. We were able to image calcium signals from 4 different depths at a frame rate of 20 Hz. A representative recording was shown in Fig. 17. In this experiment, we recorded calcium signals from four different locations of the apical dendrite (-60 µm, -100 µm, -150 µm and -220 µm below pial surface) at the same time. The result was consistent with previous observation that the largest visual evoked dendritic Ca^{2+} transients appeared on the upper part of apical dendrites. Fig. 17a demonstrated different recording sites from the cell. Fig 17b showed different trials of recording for the preferred direction and Fig. 17c gave the averaged response from different depths.

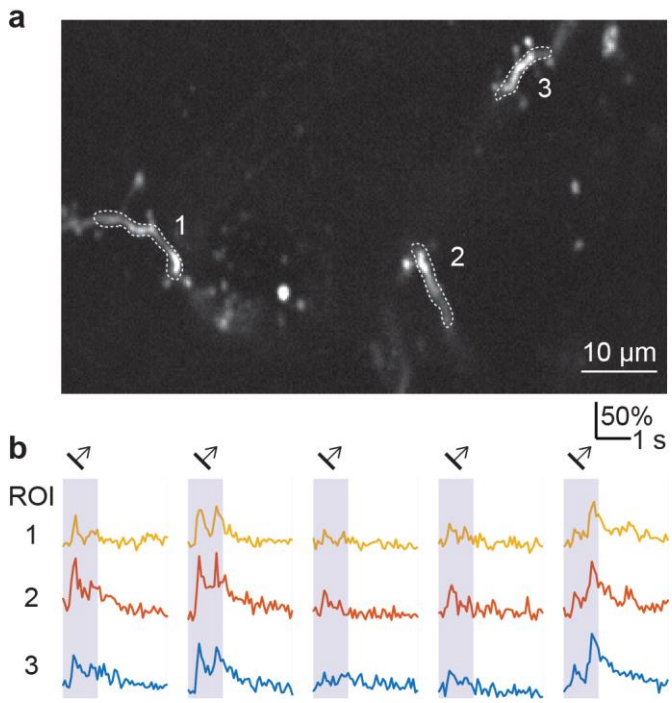

Fig. 18. Multibranch Ca^{2+} transients on tuft dendrites. a, Image showing three branches of tuft dendrites of an L4 SR neuron and ROIs on dendritic shafts. **b,** Calcium signals from ROIs specified in **a**.

Tuft dendrites of L4 pyramidal neurons usually have several branches. Therefore, we also looked at Ca^{2+} transients on different branches. Fig. 18a showed a two-photon image of the tuft dendrite which had 3 branches. Fig. 18b showed the recordings from these 3 branches. The large amplitude Ca^{2+} transients existed on all three branches.

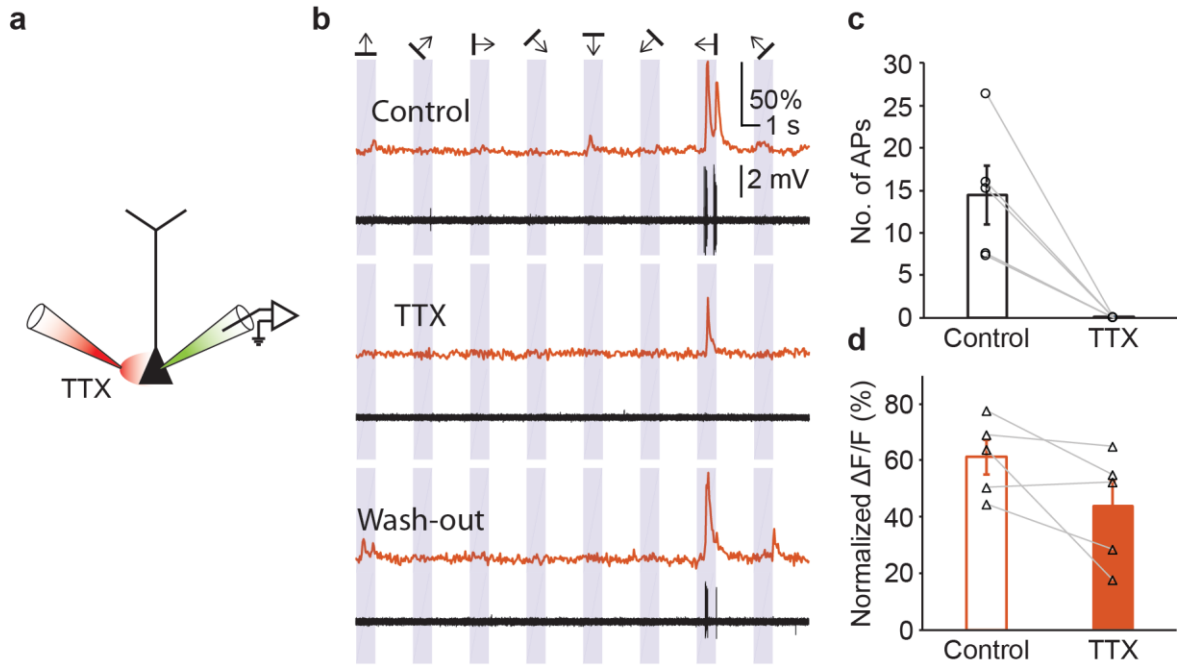

Fig. 19. Dissociation of somatic APs and dendritic calcium spikes. **a,** Scheme showing local TTX application and cell-attached recording. **b,** Representative calcium signals from tuft dendrites and somatic APs under different conditions. Red traces were calcium signals and black traces were electrophysiological recordings. **c,** Number of APs under control condition and in the presence of TTX (n = 5 neurons, $p < 0.01$, paired t-test). **d,** Normalized calcium responses under control condition and in the presence of TTX (n = 5 neurons, $p > 0.05$, paired t-test).

We were almost convinced that those large amplitude Ca^{2+} transients on tuft dendrites of L4 pyramidal neurons were local dendritic calcium spikes. We also observed that those dendritic calcium spikes were always associated with high-frequency somatic firing. Is it possible that the generation of dendritic calcium spikes relied on somatic action potentials? We sought to find a way to block somatic action potentials and see its effect on dendritic calcium spikes. A classical way to block action potentials was to use QX-314 which can block sodium channels globally from the inside of the cell. However, global blocking of sodium channel could have a great impact on the conductance of other ion channels and completely changed the excitability of neuronal membrane. The side effect was the high probability of spontaneous calcium spikes which was not observed in physiological condition. We used in our study a different approach. We applied sodium channel blocker TTX (10 μM) locally to neuronal somata from outside. The application was very local therefore the excitability of apical dendrites was not influenced. The application site was also close to action potential initiation site that local application could effectively block action potentials. To monitor

the effectiveness of action potential blocking, we performed simultaneous cell-attached recording as shown in Fig. 19a.

The results were shown in Fig. 19b. Under control condition, when no TTX was applied, the neuron responded specifically to its preferred direction of drifting gratings with somatic action potentials and dendritic calcium spikes. Local application of TTX to the soma, as expected, effectively blocked somatic action potentials, but not dendritic calcium spikes. However, dendritic calcium spikes were becoming less reliable and their amplitudes became smaller. Fig. 19c showed a summary of the data from several experiments. In all cases, action potentials were efficiently and completely blocked by local TTX application. There was only an insignificant reduction of the amplitudes of dendritic calcium spikes when somatic action potentials were blocked (Fig. 19d). These results proved that the large amplitude Ca^{2+} transients on tuft dendrites were indeed dendritic calcium spikes and they could be generated independently of somatic action potentials.

3.5 Synaptic inputs contribute to dendritic calcium spikes

The dendritic calcium spikes could be initiated by synaptic inputs if they were not generated by somatic action potentials. This was supported by the observation of visually evoked Ca^{2+} transients from spines on tuft dendrites. The recording of calcium signals from spines was possible with neurons which didn't show reliable dendritic calcium spikes. In some experiments, the contrast of visual stimulation was reduced intentionally to reduce the chance of dendritic calcium spikes. The reason is that the calcium signal from spines will be contaminated in the presence of dendritic calcium spikes. When there was a dendritic calcium spike, calcium ions in the dendritic shaft could invade into the spine head. Dendritic calcium spike could also open VGCC on spines which contributed to the extra influx of Ca^{2+} into spines.

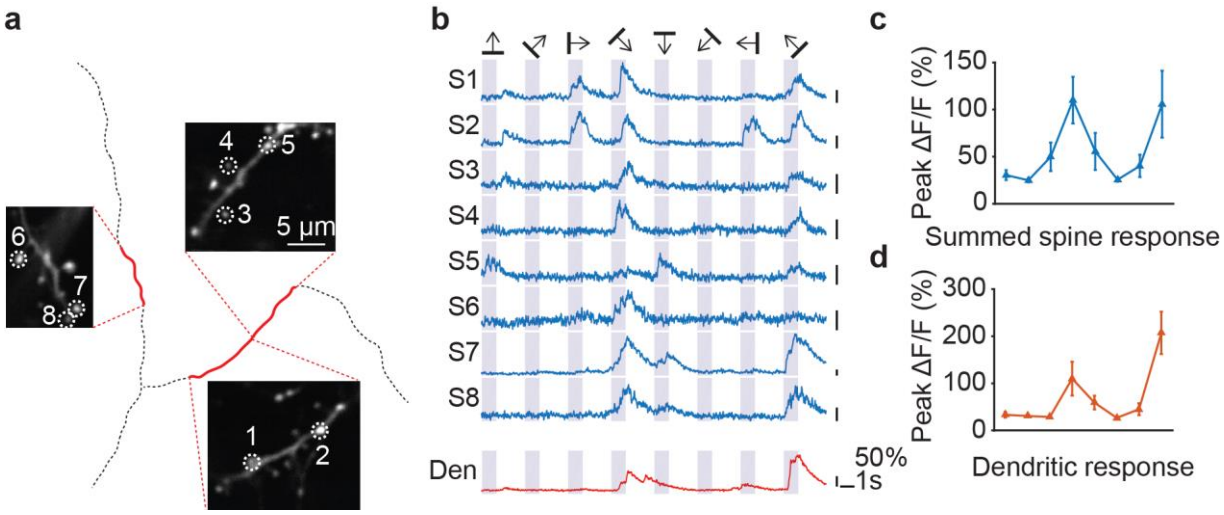

Fig. 20. Spines responses on tuft dendrites of a single L4 neuron. a, Locations of recorded spine on tuft dendrites. **b,** Averaged responses from spines shown in **a** and their dendritic shafts. **c,** Tuning curve of summed spine response. **d,** Tuning curve of averaged dendritic response.

With this approach, we recorded calcium responses from spines on tuft dendrites. Fig. 20 showed an example of recorded spine responses. Fig. 20a showed the location of recorded dendritic segments and visual responsive spines on those dendritic segments. Fig. 20b showed corresponding calcium signals from these spines and dendritic calcium spikes. We found that most visually responsive spines showed similar orientation preference as dendrites. Some spines had slightly different

preferred direction. However, when all spine responses were summed together, the averaged tuning curve was quite like that from the dendritic response (Fig. 20c, d).

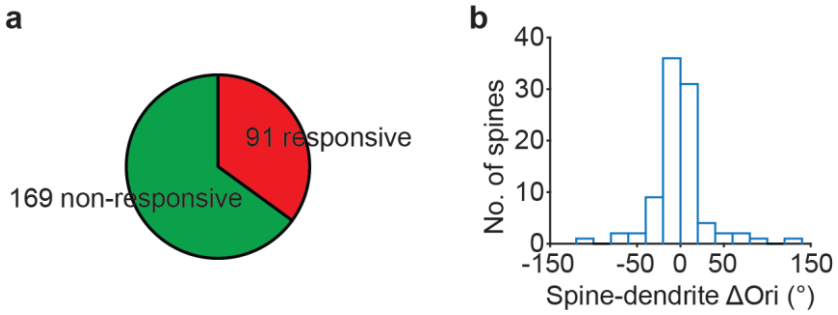

Fig. 21. Similar tuning between spines and dendrites. a, Proportion of responsive spines and nonresponsive spines (n = 280 spines from 5 neurons). **b,** Histogram showing the difference of preferred orientation between all responsive spines and their corresponding dendritic shafts.

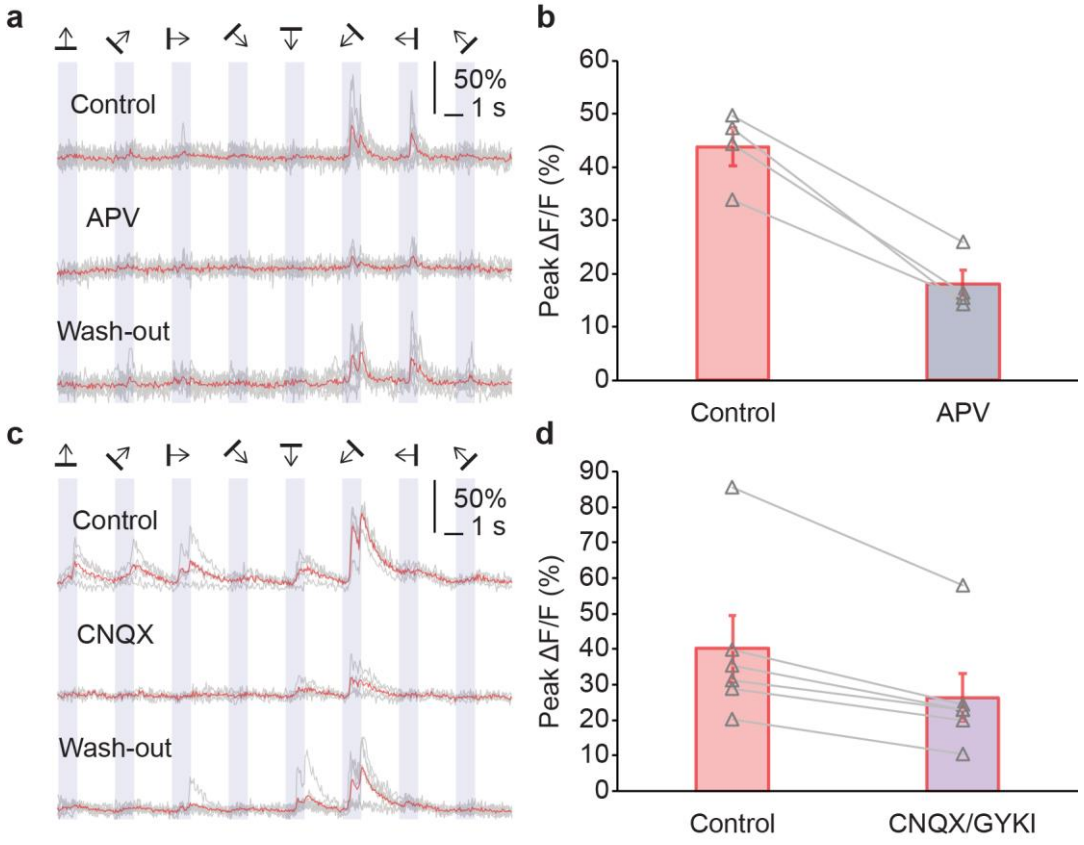

Fig. 22. Local glutamate antagonists blocked dendritic calcium spikes. a, Local application of NMDA receptor blocker APV attenuates dendritic calcium spikes. **b,** Effect of APV on dendritic calcium spikes (n = 5, $p < 0.01$, paired t-test). **c,** Local application of AMPA receptor blocker CNQX attenuates dendritic calcium spikes. **d,** Effect of CNQX or GYKI 52466 on dendritic calcium spikes (n = 6, $p < 0.01$, paired t-test). Traces are single trials (gray) and their average (red).

We recorded spines responses from 5 different neurons. In all 260 recording spines, 91 of them were visually responsive, suggesting roughly 35% of all spines on tuft dendrites are visual responsive (Fig. 21a). We calculated the difference between the preferred orientation of individual spines and dendrites. We found the previous conclusion was true for all recorded neurons. Most spines showed similar orientation preference to dendrites with very few exceptions (Fig. 21b).

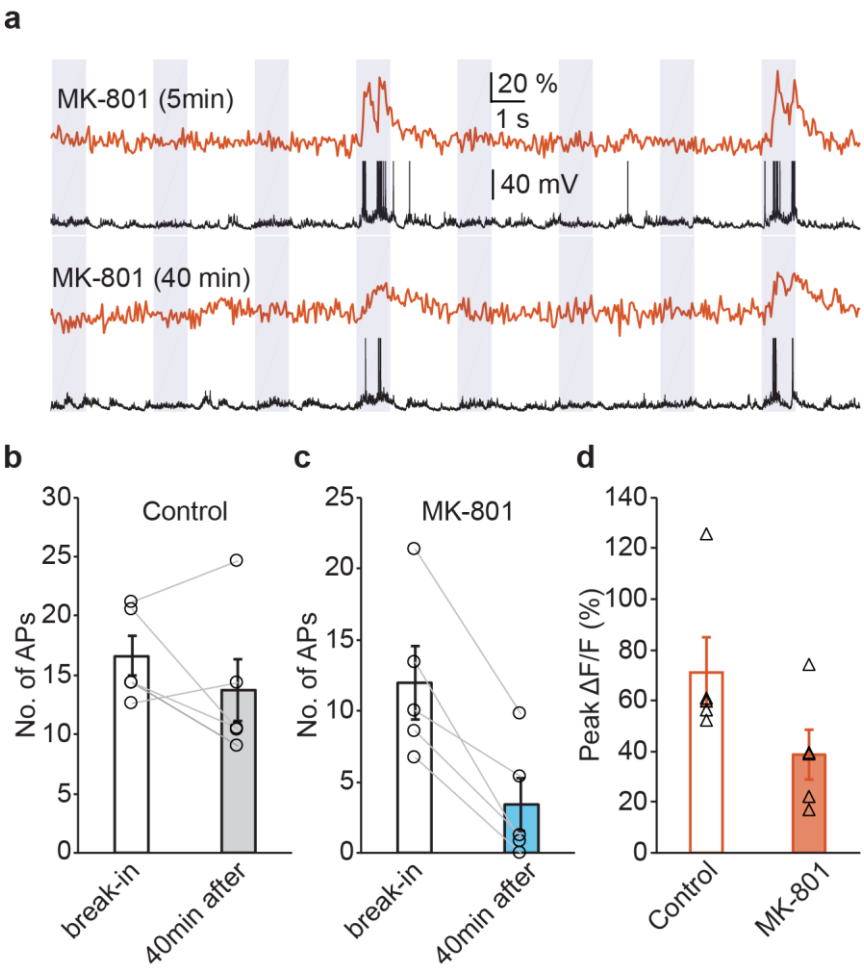

Fig. 23. Global glutamate antagonists blocked dendritic calcium spikes. a, Example recordings showing dendritic Ca^{2+} transient (red) and somatic APs (black) during whole-cell recording with MK-801. **b,** Number of APs after whole-cell break-in and 40 min after break-in under control condition (n = 5 neurons, $p > 0.05$, paired t-test). **c,** Number of APs after whole-cell break-in and 40 min after break-in in the presence of MK-801 (n = 5 neurons, $p < 0.01$, paired t-test). **d,** Amplitudes of dendritic Ca^{2+} transients under control and in the presence of MK-801 (n = 5 neurons, $p < 0.05$, two-sample t-test).

This is a strong evidence that dendritic calcium spikes were initiated by synaptic inputs on tuft dendrites. We confirmed this conclusion also by application of glutamate

antagonist (including NMDA receptors blocker APV and AMPA receptors blocker CNQX and GYKI 52466). We used 100 μM of each drug and applied them locally to tuft dendrites. We found all the drugs to be effective in blocking dendritic calcium spikes (Fig. 22). The effectiveness of APV was higher than that of CNQX/GYKI. Application of APV blocked dendritic calcium spikes completely in almost every trial (Fig. 22a, b) while CNQX/GYKI failed in some trials (Fig. 22c, d). This suggested that dendritic calcium spikes might be strongly depended on NMDA receptors.

To test whether dendritic calcium spikes were NMDA receptor-dependent we used the highly specific intracellular NMDA blocker MK-801. We performed whole-cell recordings on identified SR neurons with patch pipettes loaded with the intracellular solution containing 2 mM MK-801. At the beginning of the recording, somatic response and tuft dendritic response was not influenced as the diffusion and action of MK-801 was not immediate. 40 minutes after the break-in, the somatic response was partially blocked as well as tuft dendritic response (Fig. 23a). In control experiments, without MK-801 inside pipette solution, there was no significant reduction in somatic response (Fig. 23b). However, with the presence of MK-801, there was a strong reduction of somatic responses (Fig. 23c). The amplitudes of dendritic calcium spikes in the presence of MK-801 were also significantly smaller than that under control condition (Fig. 23d).

3.6 Dendritic calcium spikes determine the output of SR neurons

The exact function of dendritic calcium spikes was still not completely clear. Possible roles in amplification of distal inputs, coincidence detection, and long-term potentiation have been shown in many in vitro studies. Its function *in vivo* was started to be revealed only recently.

During our experiments, dendritic calcium spikes were mostly found on SR neurons-neurons that exhibited a particularly strong response to visual stimulation. The likely explanation is that dendritic calcium spikes endue neurons with super responsiveness. In this part of the study, we will explore the possibility of this hypothesis with the following methods.

We observed that dendritic calcium spikes were associated with high-frequency somatic action potentials. The number of action potentials during visual stimulation was always larger when there was a large amplitude dendritic calcium spike. Conversely, the number of action potentials is small when the dendritic calcium spike is small or absent (Fig. 24a and 24b). Further analysis showed that the amplitudes are linearly correlated with the number of action potentials in a single neuron (Fig. 24c).

In the population level, our analysis showed that dendritic calcium spikes were indicators of SR neurons. We pooled data from weakly responsive neurons and SR neurons together and analyzed the relationship between the number of action potentials and the amplitude of dendritic calcium spikes. We found that neurons responding with less than 10 action potentials to preferred direction have no or very small dendritic calcium spikes while neurons responding with more than 20 action potentials all have large amplitude dendritic calcium spikes (Fig. 24d).

There is indeed a strong correlation between dendritic calcium spikes and super responsiveness. Can dendritic calcium spikes really enhance somatic responses? To prove this, we need to intervene dendritic calcium spikes and see its effects on somatic firing. The previous MK-801 experiment partly supported this idea as somatic firing was strongly reduced after blocking NMDA conductance (Fig. 23). The shortcoming of this experiment was that it showed a global effect from many dendrites instead of local effect from tuft dendrites.

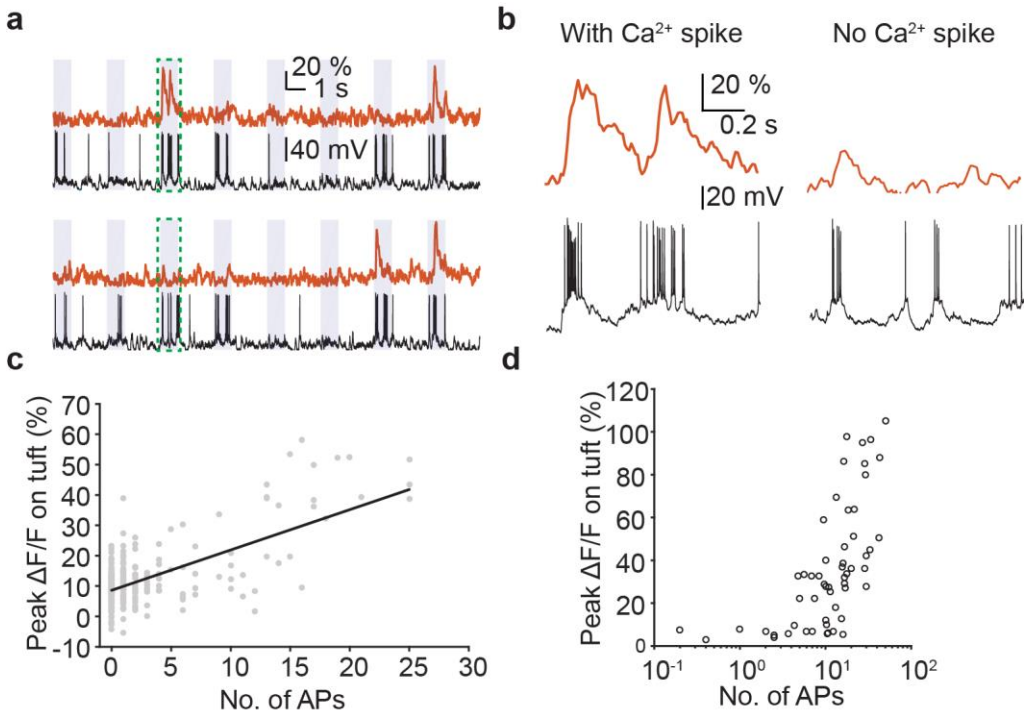

Fig. 24. Correlation between dendritic calcium spikes and somatic APs. a, Representative recordings of Ca^{2+} transients (red) and somatic APs (black) with and without dendritic calcium spikes. **b,** Magnification of recordings in green boxes in **a**. **c,** Correlation between amplitude of dendritic calcium spikes and number of APs for the neuron in **a** (n = 10 trials, r = 0.56, p < 0.001, Spearman's rank test). **d,** Correlation between amplitude of dendritic calcium spikes and number of APs for all recorded neurons (n = 58 neurons, r = 0.72, p < 0.001, Spearman's rank test).

Baclofen as a type B GABA receptor agonist was shown to be effective in blocking dendritic calcium spikes of layer 5 pyramidal neurons when applied locally (Pérez-Garci et al., 2013). Therefore, it is the ideal agent to test our hypothesis. We used 100 µM baclofen and applied locally to tuft dendrites (Fig. 25a). Not surprisingly, dendritic calcium spikes on the tuft dendrites were completely blocked (Fig. 25b and c).

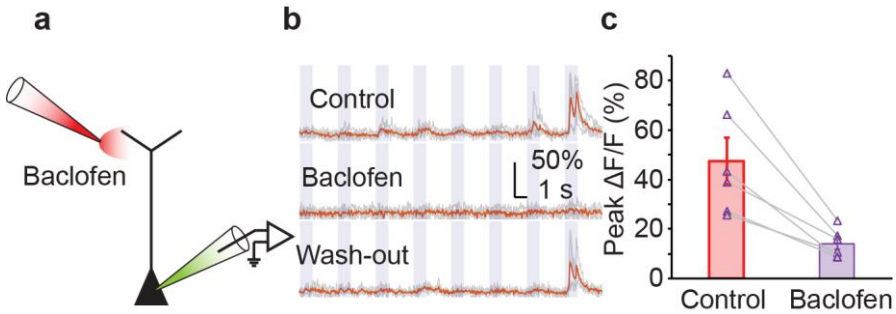

Fig. 25. Local application of baclofen blocked dendritic calcium spikes. a, Scheme showing local baclofen application and cell-attached recording. **b,** Representative dendritic Ca^{2+} transients under different conditions. Traces are single trials (gray) and their average (red). **c,** Amplitudes of dendritic Ca^{2+} transients under different conditions (n = 7 neurons, p < 0.01, paired t-test).

Next, we wanted to know its effect on somatic action potentials. We again did simultaneous cell-attached recording and dendritic calcium imaging. With the local application of baclofen on tuft dendrites, dendritic calcium spikes in response to the preferred direction of drifting grating were completely blocked. Along with this was the drastic decrease in somatic firing. This is not the case when no baclofen was applied, or when baclofen was washed out (Fig. 26a). For non-preferred directions of drifting grating, there was no dendritic calcium spikes and fewer numbers of somatic action potentials. Hence the effect of baclofen is also weaker (Fig. 26b).

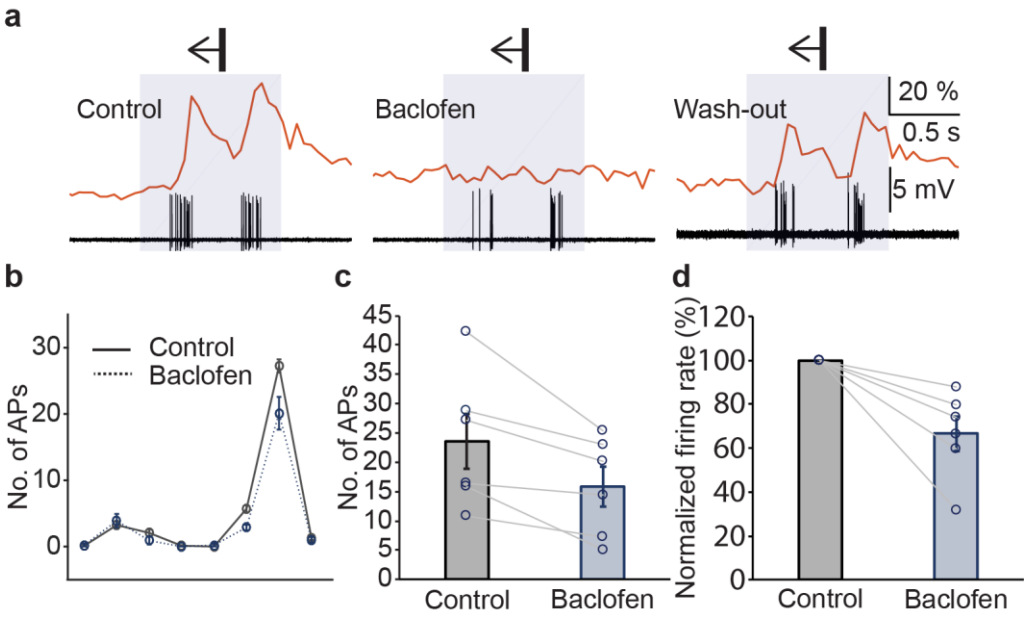

Fig. 26. Baclofen application reduced somatic responses to preferred directions. a, Ca^{2+} transients (red) and somatic APs (black) in response to preferred direction under different conditions. **b,** Tuning curve of somatic APs under control and baclofen conditions. **c,** Frequency of APs to the preferred direction under control and baclofen conditions (n = 6 neurons, $p < 0.01$, paired t-test). **d,** Normalized firing rate under control and baclofen conditions (n = 6 neurons, $p < 0.01$, paired t-test).

For all the neurons tested with baclofen, a reliable reduction of somatic action potentials in response to the preferred direction of drifting grating was observed (Fig. 26c). Since the firing rate of recorded neurons spanned a large range, we normalized the firing rate to see a population effect. The reduction of somatic was determined to be ~30% on average when dendritic calcium spike was blocked by baclofen (Fig. 26c).

Therefore, we proved that dendritic calcium spikes on tuft dendrites were very important in determining super responsiveness of L4 pyramidal neurons. It was

initiated by synaptic inputs on tuft dendrites in L1, benefited mostly from NMDA conductance and enhanced somatic firing for preferred directions of drifting gratings.

3.7 Highly tuned LGN inputs in layer 1 of V1

In the last part of our study, we tried to investigate the source of orientation select inputs in L1 of primary visual cortex. One of the possible sources is dLGN. It was demonstrated by histology study that dLGN sent most axons to layer 4 of V1 and there was also a substantial number of axons in layer 1. A recent study showed that direction selective retinal ganglion cells projected to dLGN and finally targeted layer 1. This dedicated retino-geniculo-cortical pathway was found to provide layer 1 with orientation and direction selective inputs (Cruz-Martín et al., 2014).

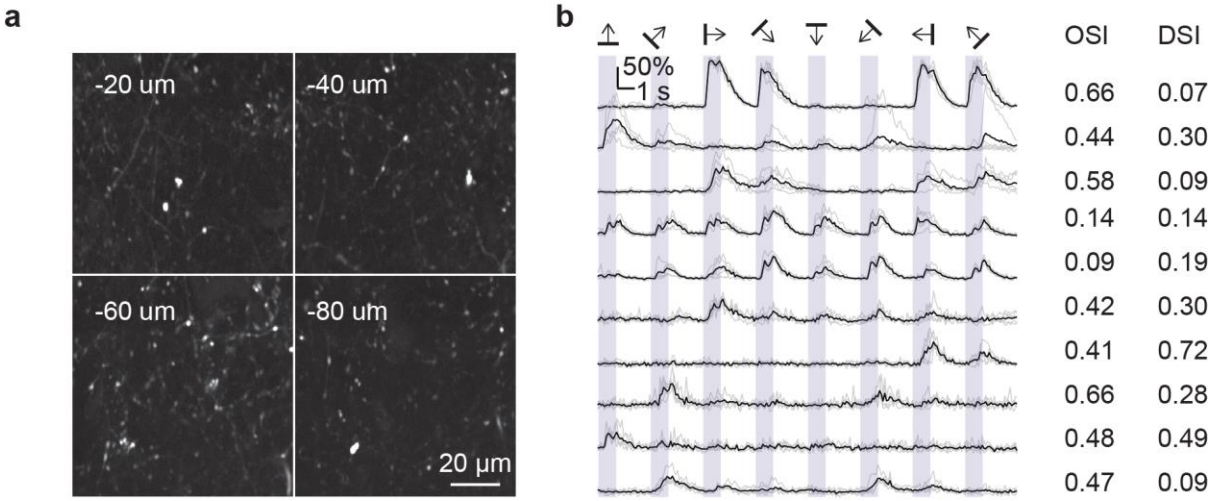

Fig. 27. Imaging of axonal boutons from LGN in layer 1 of V1. a, Two-photon images of GCaMP6s labeled axonal boutons in layer 1. **b,** Representative response of axonal boutons. Traces are single trials (gray) and their average (black).

To confirm this and more recent findings from other researchers, we performed calcium imaging of axonal boutons in layer 1 of V1 and quantified their responses. Axonal boutons were labeled by injecting GCaMP6s virus in dLGN. We recorded boutons responses from different depths of layer 1 and found the existence of orientation and direction selective boutons (Fig. 27). Images of labeled axonal boutons were shown in Fig. 27a. Typical responses from axonal boutons were shown in Fig. 27b. Tuning properties of boutons in layer 1 including preferred orientations, gOSI and DSI were consistent with previous studies (Fig. 28). Compared with L4 neurons, axonal boutons in layer 1 had similar orientation tuning (median: 0.26; see Fig. 7a and Fig. 28b) but less direction tuning (median: 0.19; see Fig. 7b and Fig. 28c). The

preferred orientation of axonal boutons in layer 1 was also biased to the vertical orientation (Fig. 28a).

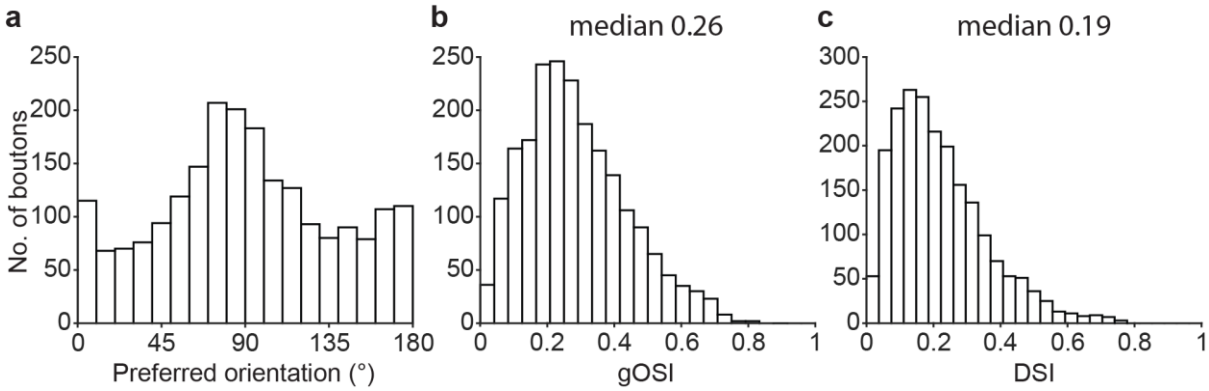

Fig. 28. Tuning properties of axonal boutons in layer 1. a, Distribution of preferred orientations. **b,** Distribution of gOSI. **c,** Distribution of DSI.

These findings supported the hypothesis that a dedicated circuit might exist and provide orientation and direction inputs in layer 1. It might contribute to the tuned inputs on tuft dendrites of layer 4 neurons. Of course, further evidence like the existence of functional synapses between dLGN boutons and spines on tuft dendrites is urgently needed to confirm this hypothesis.

4 Discussion

This thesis explored cellular and circuit mechanisms of orientation selectivity in layer 4 of mouse V1 with the help of *in vivo* two-photon calcium imaging and together with several technical developments. These developments include (1) dendritic calcium imaging on functionally defined neurons by using a two-step approach; (2) multiple-plane imaging for studying dendritic function in three dimensions; (3) light anesthesia for dendritic calcium imaging.

The results indicate non-uniformity in response strength of individual orientation selective L4 neuron. Among all orientation selective L4 neurons, a small population exhibited particularly large response amplitudes and were defined as super responsive neurons (SR neuron). On these SR neurons, reliable dendritic calcium spikes were observed in their L1 dendritic tufts. These dendritic calcium spikes were NMDA receptor-dependent and were evoked by similarly tuned single spine inputs on L1 dendrites. Most importantly, the dendritic calcium spikes were found to enhance the output of the neuron.

4.1 Technical developments and considerations

4.1.1 Neuronal population staining

Labeling neuronal population with a synthetic Ca^{2+} indicator by MCBL method has become a powerful way to monitor the activity of neuronal population *in vivo* since its invention (Stosiek et al., 2003). Typically, this method uses OGB1 in AM ester form to stain neurons in the range of 300-500 µm. However, the imaging from deeper than 300 µm below pia was usually with a low signal-to-noise ratio (SNR). This low SNR makes this method not suitable for deep tissue imaging for the following two reasons. First, the short wavelength excitation light and emission light of OGB1 (920 nm and 523 nm) are easily scattered by brain tissue, especially by blood vessels. This sub-optimal fluorophore excitation and ineffective emission photon collection make calcium signal weaker. Second, the two-photon microscope has a worse resolution in z-axis. The imaging is contaminated by out of focus fluorescence signal if the stained area is too large in z-axis, and therefore the background noise is higher.

MCBL method has been recently improved for deep brain imaging by using a new red-shifted Ca^{2+} indicator Cal-590 and achieving localized brain tissue staining (Tischbirek et al., 2015). Cal-590 has longer two-photon excitation and emission wavelength (1050 nm and 588 nm). Light with longer wavelength penetrates the tissue more easily and scatters less. Localized staining means staining is restricted to the expected range of imaging depths (-350 µm to -450 µm below pia) rather than a much larger volume in the brain. Most importantly, staining above the imaging depths should be avoided. By this mean, contamination from out of focus fluorescence will be minimized. In addition, the red-shifted calcium indicator Cal-590 has a much lower affinity (K_d: ~561 nM) for calcium ions and thus can maintain better linearity to a larger number of action potentials than the previously widely used green calcium indicator OGB-1 AM (K_d: ~170 nM).

4.1.2 Functional targeted single-cell electroporation

Targeted single-cell electroporation was widely used to deliver large molecules like DNAs and RNAs *in vitro* and *in vivo* (Bestman et al., 2006; Haas et al., 2001). This

method was later proved to be useful for loading single cells with Ca^{2+} indicator OGB1-6k *in vivo* (Nevian and Helmchen, 2007). It allowed *in vivo* functional imaging of Ca^{2+} dynamics in subcellular compartments like spines and dendrites with a low background. The advantage of this method is that it is much more efficient than staining single cells with sharp electrodes (Helmchen et al., 1999) and patch pipettes (Helmchen and Waters, 2002).

In this study, we combined this method with Cal-590 AM based MCBL to label identified SR neurons and study their dendritic property. There were multiple aspects in determining the success rate of electroporation. For example, the concentration of OGB1-6k inside electroporation solution should not be too high. Originally, 1 mM OGB1-6k was used for electroporation which resulted in ~200 μM intracellular dye concentration (Nevian and Helmchen, 2007). Other studies used much higher dye concentration (Hill et al., 2013; Jia et al., 2014). In theory, electroporation with a higher concentration of OGB1-6k might increase the chance of successful filling of the neuron but could easily overfill the neuron with Ca^{2+} indicators. Other aspects include the amplitude and the duration of electroporation pulses, the position of the pipette tip relative to the target neuron, and so on.

4.1.3 Anesthesia

In this study, we used a light anesthesia (combination of chlorprothixene and low concentration isoflurane) preparation to investigate the responsive properties of L4 neurons in mouse V1. Light anesthesia could provide enough stability for dendritic calcium imaging while maintaining a strong visually evoked response.

Isoflurane was known to suppress spontaneous and visually evoked neuronal activity (Adelsberger et al., 2005; Raz et al., 2014; Villeneuve and Casanova, 2003), probably because of its action on $GABA_A$ and glycine receptors (Grasshoff and Antkowiak, 2006). In particular, visually evoked neuronal response (Durand et al., 2016; Niell and Stryker, 2010; Vaiceliunaite et al., 2013), synaptic activity (Haider et al., 2013) and dendritic response (Potez and Larkum, 2008) were highly dependent on animal states. Previous studies performing dendritic calcium imaging with deeply anesthetized animals showed weak response and might suffer from these side effects (Chen et al., 2011; Jia et al., 2010). In pilot experiments, we observed that visually evoked neuronal

response in awake animals was indeed much stronger and more reliable than that in deeply anesthetized animals. Ideally, it is better to perform experiments with awake animals, but even tiny movement of the animal during experiments make it impossible to image small structures like dendrites and spines. However, we found the response recorded in lightly anesthetized animals very close to that in awake animals. In other studies, robust visual responses was also found in lightly anesthetized animals (Kaneko et al., 2008; Piscopo et al., 2013; Smith and Häusser, 2010). It should be noted that the response in light anesthesia was still not identical to awake condition as shown previously (Haider et al., 2013).

4.2 Visual response properties in layer 4 of mouse V1

4.2.1 Emergence of orientation selectivity in L4 neurons

The mechanism for generating orientation selectivity in the mammalian V1 has been the central question in understanding cortical information processing. In the classical model proposed by Hubel & Wiesel based on cat visual system, the LGN relay cells are not tuned for orientations but have circular receptive fields. The orientation selectivity of L4 simple cells emerges from the arrangement of such untuned thalamic inputs (Hubel and Wiesel, 1962). However, this model is oversimplified, and its generality has been challenged by new findings.

Early studies have already identified orientation selective neurons in layer 4 of mouse V1. They were shown to be less common in layer 4 than in layer 2/3 (Mangini and Pearlman, 1980; Metin et al., 1988). A recent study found that the mean orientation selectivity of L4 neurons was similar to that of neurons in layer 2/3 (Niell and Stryker, 2008). More recent studies using calcium imaging also confirmed the existence of a large fraction of orientation selective neurons in layer 4 (Kondo and Ohki, 2015; Sun et al., 2015). This discrepancy can be attributed to the improvement in recording technique and analysis method. We know that layer 5 neurons and interneurons are not highly tuned, they also have very large extracellular spikes and high firing rates. The possibility was that in those early studies, researchers could not remove the contamination of these two sets of neurons from their extracellular recordings.

After identification of orientation selective neurons in layer 4, the next question is how does orientation selectivity emerge in layer 4 of mouse V1? Does Hubel & Wiesel model still apply in mouse V1? Regarding this question, several potential mechanisms have been proposed. In the study of Scholl et al, they identified a high degree of orientation selectivity in LGN relay cells and this orientation selectivity was independent of cortical feedback connections. From this point, they believed that orientation selectivity in mouse V1 (including layer 4) was inherited from LGN (Scholl et al., 2013). An earlier study by Piscopo et al also confirmed the orientation selectivity of LGN cells (Piscopo et al., 2013). In a study from Lien and Scaziani, they found that thalamic excitation to L4 neurons is organized into spatially offset, yet highly overlapping, ON and OFF receptive fields and thalamic excitation contributed only 30%

to the total excitation (Lien and Scanziani, 2013). They excluded the possibility that the tuning of thalamic excitation was from orientation- and direction-selective neurons in LGN. The study from Li et al using similar cortex silencing method found that thalamic excitation was orientation and direction selective. This tuned thalamic inputs were further linearly amplified by intracortical circuits (Li et al., 2013). Sun et al recently improved the two-photon microscope with adaptive optics. They investigated the response properties of axonal boutons from LGN in mouse V1 (Sun et al., 2015). They found that half of the boutons in layer 4 were orientation tuned and their orientation and direction biases matched that of L4 neurons. Their data suggested that the selectivity of neurons in V1 was inherited from tuned thalamic inputs. Kondo and Ohki used a similar strategy to record the response of axonal boutons from LGN in V1. They did not use adaptive optics but measured and improved point spread function (PSF). Their data showed that axonal boutons in layer 4 were less tuned than axonal boutons in more superficial layers in V1. They proposed that V1 neurons might not simply inherit selectivity from LGN inputs (Kondo and Ohki, 2015).

In our study, we focused on synaptic inputs on tuft dendrites of L4 neurons. We found that spine responses on tuft dendrites are highly orientation and direction selective. The preferred orientation of those tuned spines was biased to the preferred orientation of the corresponding L4 neuron. Due to technical reasons, we could not record responses from spines on basal dendrites in layer 4 with a good signal to noise ratio at the moment. We could not make a conclusion about what kind of inputs were received by basal dendrites in layer 4. On the other hand, our data suggested that the tuft dendrites of L4 neurons received highly tuned inputs in superficial layers especially in layer 1. Those highly tuned inputs probably came from LGN based on previous studies (Cruz-Martín et al., 2014; Kondo and Ohki, 2015; Sun et al., 2015) and our recordings on LGN axonal boutons in layer 1.

4.2.2 Response strength of orientation selective L4 neurons

In our study, we found that the response strength of L4 neurons was not uniform but with a small number of neurons showing much larger responses. The skewed distribution of response strength was also found previously in the higher visual area of macaque (Yang and Maunsell, 2004). In fact, many biological parameters were found

to have a lognormal distribution rather than a normal distribution (Buzsáki and Mizuseki, 2014). This observation suggested that a small portion of neurons might perform most of the tasks during sensory information processing. The idea was also supported by sparse coding theory that a small number of active neurons was used to encode sensory information at any given time point (Olshausen and Field, 2004).

4.3 Dendritic calcium spikes in L4 neurons of mouse V1

4.3.1 Dendritic spikes in visual cortex *in vivo*

Dendritic spikes have been investigated extensively *in vitro* (Amitai et al., 1993; Schiller et al., 1997, 2000; Stuart et al., 1997). However, whether the dendritic spike is a universal dendritic mechanism for synaptic integration *in vivo* is still unclear. Our study identified dendritic calcium spikes on the tuft dendrites of layer 4 neurons in mouse V1 *in vivo*. The dendritic calcium spikes were observed on what we called super responsive neurons. The experiments were carried out with lightly anesthetized animals which had similar visual evoked responses as in awake animals.

There are several differences between *in vitro* and *in vivo* preparations. Firstly, there are lots of spontaneous and evoked synaptic activities *in vivo*. These activities may completely change the resting membrane potential, input resistance and the effective membrane time constant of the cell and dendrites (Steriade, 2001). Secondly, the pattern of synaptic inputs on the dendritic tree under physiological conditions is unclear. There were not so many studies on this. Anatomical evidence suggested that synaptic inputs have a non-uniform distribution on dendritic trees (Felleman and Van Essen, 1991). The study from Chen et al demonstrated that in deeply anesthetized mice, more than 500 active spines were required for generating an up state (Chen et al., 2013). Lastly, synaptic activities are greatly influenced by surrounding neurons and glia cells (Zorec et al., 2012). Even all studies can be performed in vivo, synaptic activities are also influenced by the animal states like anesthesia, wakefulness and so on.

Dendritic spikes were recorded under *in vivo* condition in many studies. However, most studies were restricted to somatosensory cortex (Gambino et al., 2014; Larkum and Zhu, 2002; Lavzin et al., 2012; Murayama et al., 2009; Palmer et al., 2014; Xu et al., 2012) and hippocampus (Bittner et al., 2015; Grienberger et al., 2014; Sheffield and Dombeck, 2015). Different sensory or behavior paradigms probably utilize dendritic spikes differently, therefore it is easy to observe dendritic spikes in some cortical areas and in some types of neurons.

Recent *in vivo* studies in several sensory cortical areas did not report any form of dendritic spikes (Chen et al., 2011; Jia et al., 2010; Varga et al., 2011). There are several possible reasons for this. First, animals in those studies were deeply

anesthetized and this could greatly suppress sensory evoked neuronal responses. Second, the membrane potentials of the recorded neurons in those studies were hyperpolarized which could also suppress dendritic spikes. Third, neurons recorded in those studies were weakly responsive neurons in which dendritic spikes could not be generated. Forth, different types of neurons utilized different mechanism to integrate synaptic inputs. Some neurons used the linear way of synaptic integration and other neurons used the non-linear way like dendritic spikes.

Until now there was only one study that reported dendritic spikes in visual cortex *in vivo* (Smith et al., 2013). The author performed dendritic patch-clamp recordings from layer 2/3 neurons in the mouse V1 and found orientation selective dendritic spikes. These dendritic spikes are NMDA receptor-dependent local regenerative events that also contain dendritic sodium spikes. The recordings were acquired from both lightly anesthetized and awake mice and were not biased by the influence of anesthesia.

4.3.2 Function of dendritic spikes

In the current study, we found that dendritic calcium spikes were particularly associated with high-frequency somatic action potentials. We speculated that somatic output was enhanced in those neurons by dendritic calcium spikes. We performed several tests to verify this hypothesis. First, we analyzed the relationship between the amplitude of dendritic calcium spikes and the number of somatic action potentials. The result showed that they were highly correlated. Second, we performed whole-cell recording with NMDA receptor blocker MK-801. With the blocking of NMDA receptors, the amplitude of dendritic spikes decreased significantly. At the same time, the number of somatic action potentials decreased significantly. Third, we blocked the dendritic calcium spikes locally with baclofen which also reduced somatic action potentials significantly.

An important question in dendritic research is to determine the functions of dendritic spikes. There were different theories and debates on this topic. One leading theory is that dendritic spikes allow neurons to respond to coincident activation of multiple dendritic domains. As a result of coincident activation, a dendritic spike can enhance action potential firing in the axon. Another theory is that dendritic spikes can mediate synaptic plasticity. There was also a theory stating that dendritic spikes can amplify

distal synaptic inputs (Spruston et al., 2013). In the live brain, the situation could be much more complicated than a simple theory. Dendritic spikes could have different functions in different brain regions and different cell types. It is also possible that dendritic spikes have different functions in different dendritic compartments of a single cell. *In vitro* studies classified dendritic spikes into three types. In an operational neural circuit, dendritic spikes could be the combination of these three types. The function will be determined by the ratio of different channels involved.

5 Bibliography

Adelsberger, H., Garaschuk, O., and Konnerth, A. (2005). Cortical calcium waves in resting newborn mice. Nat. Neurosci. *8*, 988–990.

Amitai, Y., Friedman, A., Gutnick, M.J., and Connors, B.W. (1993). Regenerative activity in apical dendrites of pyramidal cells in neocortex. Cereb. Cortex *3*, 26–38.

Araya, R., Eisenthal, K.B., and Yuste, R. (2006). Dendritic spines linearize the summation of excitatory potentials. Proc. Natl. Acad. Sci. U. S. A. *103*, 18799–18804.

Bestman, J.E., Ewald, R.C., Chiu, S.-L., and Cline, H.T. (2006). In vivo single-cell electroporation for transfer of DNA and macromolecules. Nat. Protoc. *1*, 1267–1272.

Bickford, M.E., Zhou, N., Krahe, T.E., Govindaiah, G., and Guido, W. (2015). Retinal and Tectal "Driver-Like" Inputs Converge in the Shell of the Mouse Dorsal Lateral Geniculate Nucleus. J. Neurosci. *35*, 10523–10534.

Bittner, K.C., Grienberger, C., Vaidya, S.P., Milstein, A.D., Macklin, J.J., Suh, J., Tonegawa, S., and Magee, J.C. (2015). Conjunctive input processing drives feature selectivity in hippocampal CA1 neurons. Nat. Neurosci. *18*, 1–13.

Brainard, D.H. (1997). The Psychophysics Toolbox. Spat. Vis. *10*, 433–436.

Buzsáki, G., and Mizuseki, K. (2014). The log-dynamic brain: how skewed distributions affect network operations. Nat. Rev. Neurosci. *15*, 264–278.

Chen, X., Leischner, U., Rochefort, N.L., Nelken, I., and Konnerth, A. (2011). Functional mapping of single spines in cortical neurons in vivo. Nature *475*, 501–505.

Chen, X., Leischner, U., Varga, Z., Jia, H., Deca, D., Rochefort, N.L., and Konnerth, A. (2012). LOTOS-based two-photon calcium imaging of dendritic spines in vivo. Nat. Protoc. *7*, 1818–1829.

Chen, X., Rochefort, N.L., Sakmann, B., and Konnerth, A. (2013). Reactivation of the Same Synapses during Spontaneous Up States and Sensory Stimuli. Cell Rep. *4*, 31–39.

Colgan, L.A., and Yasuda, R. (2014). Plasticity of Dendritic Spines: Subcompartmentalization of Signaling. Annu. Rev. Physiol. *76*, 365–385.

Cruz-Martín, A., El-Danaf, R.R.N., Osakada, F., Sriram, B., Dhande, O.O.S., Nguyen, P.P.L., Callaway, E.E.M., Ghosh, A., and Huberman, A.A.D. (2014). A dedicated circuit links direction-selective retinal ganglion cells to the primary visual cortex. Nature *507*, 358–361.

Dräger, U.C. (1974). Autoradiography of tritiated proline and fucose transported transneuronally from the eye to the visual cortex in pigmented and albino mice. Brain Res. *82*, 284–292.

Dräger, U.C., and Drager, U.C. (1975). Receptive fields of single cells and topography in mouse visual cortex. J. Comp. Neurol. *160*, 269–290.

Durand, S., Iyer, R., Mizuseki, K., de Vries, S., Mihalas, S., and Reid, R.C. (2016). A Comparison of Visual Response Properties in the Lateral Geniculate Nucleus and Primary Visual Cortex of Awake and Anesthetized Mice. J. Neurosci. *36*, 12144–12156.

Fan, J., Woodruff, M.L., Cilluffo, M.C., Crouch, R.K., and Fain, G.L. (2005). Opsin activation of transduction in the rods of dark-reared Rpe65 knockout mice. J. Physiol. *568*, 83–95.

Felleman, D.J., and Van Essen, D.C. (1991). Distributed hierachical processing in the primate cerebral cortex. Cereb. Cortex *1*, 1–47.

Gambino, F., Pagès, S., Kehayas, V., Baptista, D., Tatti, R., Carleton, A., and Holtmaat, A. (2014). Sensory-evoked LTP driven by dendritic plateau potentials in vivo. Nature *515*, 116–119.

Grasshoff, C., and Antkowiak, B. (2006). Effects of isoflurane and enflurane on GABAA and glycine receptors contribute equally to depressant actions on spinal ventral horn neurones in rats. Br. J. Anaesth. *97*, 687–694.

Grienberger, C., Chen, X., and Konnerth, A. (2014). NMDA receptor-dependent multidendrite Ca2+ spikes required for hippocampal burst firing invivo. Neuron *81*, 1274–1281.

Grienberger, C., Chen, X., and Konnerth, A. (2015). Dendritic function in vivo. Trends Neurosci. *38*, 45–54.

Grubb, M.S., and Thompson, I.D. (2003). Quantitative characterization of visual response properties in the mouse dorsal lateral geniculate nucleus. J. Neurophysiol.

90, 3594–3607.

Guizar-Sicairos, M., Thurman, S.T., and Fienup, J.R. (2008). Efficient subpixel image registration algorithms. Opt. Lett. *33*, 156–158.

Haas, K., Sin, W.C., Javaherian, A., Li, Z., and Cline, H.T. (2001). Single-cell electroporation for gene transfer in vivo. Neuron *29*, 583–591.

Haider, B., Häusser, M., and Carandini, M. (2013). Inhibition dominates sensory responses in the awake cortex. Nature *493*, 97–100.

Helmchen, F., and Waters, J. (2002). Ca2+ imaging in the mammalian brain in vivo. Eur. J. Pharmacol. *447*, 119–129.

Helmchen, F., Svoboda, K., Denk, W., and Tank, D.W. (1999). In vivo dendritic calcium dynamics in deep-layer cortical pyramidal neurons. Nat. Neurosci. *2*, 989–996.

Hering, H., and Sheng, M. (2001). DENDRITIC SPINES: STRUCTURE, DYNAMICS AND REGULATION. Nat. Rev. Neurosci. *2*, 880–888.

Hill, D.N., Varga, Z., Jia, H., Sakmann, B., and Konnerth, A. (2013). Multibranch activity in basal and tuft dendrites during firing of layer 5 cortical neurons in vivo. Proc. Natl. Acad. Sci. U. S. A. *2013*, 13618–13623.

Hubel, D.H., and Wiesel, T.N. (1959). Receptive fields of single neurones in the cat's striate cortex. J. Physiol. *148*, 574–591.

Hubel, D.H., and Wiesel, T.N. (1962). Receptive fields, binocular interaction and functional architecture in the cat's visual cortex. J. Physiol. *160*, 106–154.2.

Iacaruso, M.F., Gasler, I.T., and Hofer, S.B. (2017). Synaptic organization of visual space in primary visual cortex. Nature *547*, 449–452.

Jia, H., Rochefort, N.L., Chen, X., and Konnerth, A. (2010). Dendritic organization of sensory input to cortical neurons in vivo. Nature *464*, 1307–1312.

Jia, H., Varga, Z., Sakmann, B., and Konnerth, A. (2014). Linear integration of spine Ca2+ signals in layer 4 cortical neurons in vivo. Proc. Natl. Acad. Sci. U. S. A. *111*, 9277–9282.

Judkewitz, B., Rizzi, M., Kitamura, K., and Häusser, M. (2009). Targeted single-cell electroporation of mammalian neurons in vivo. Nat. Protoc. *4*, 862–869.

Kaneko, M., Hanover, J.L., England, P.M., and Stryker, M.P. (2008). TrkB kinase is required for recovery, but not loss, of cortical responses following monocular deprivation. Nat. Neurosci. *11*, 497–504.

Kitamura, K., Judkewitz, B., Kano, M., Denk, W., and Häusser, M. (2008). Targeted patch-clamp recordings and single-cell electroporation of unlabeled neurons in vivo. Nat. Methods *5*, 61–67.

Koch, C., Poggio, T., and Torre, V. (1983). Nonlinear interactions in a dendritic tree: localization, timing, and role in information processing. Proc. Natl. Acad. Sci. U. S. A. *80*, 2799–2802.

Koester, H.J., and Sakmann, B. (1998). Calcium dynamics in single spines during coincident pre- and postsynaptic activity depend on relative timing of back-propagating action potentials and subthreshold excitatory postsynaptic potentials. Proc. Natl. Acad. Sci. U. S. A. *95*, 9596–9601.

Kondo, S., and Ohki, K. (2015). Laminar differences in the orientation selectivity of geniculate afferents in mouse primary visual cortex. Nat. Neurosci. *19*, 1–6.

Krahe, T.E., El-Danaf, R.N., Dilger, E.K., Henderson, S.C., and Guido, W. (2011). Morphologically Distinct Classes of Relay Cells Exhibit Regional Preferences in the Dorsal Lateral Geniculate Nucleus of the Mouse. J. Neurosci. *31*, 17437–17448.

Larkum, M.E., and Zhu, J.J. (2002). Signaling of layer 1 and whisker-evoked Ca2+ and Na+ action potentials in distal and terminal dendrites of rat neocortical pyramidal neurons in vitro and in vivo. J. Neurosci. *22*, 6991–7005.

Lavzin, M., Rapoport, S., Polsky, A., Garion, L., and Schiller, J. (2012). Nonlinear dendritic processing determines angular tuning of barrel cortex neurons in vivo. Nature *490*, 397–401.

Li, Y., Ibrahim, L.A., Liu, B., Zhang, L.I., and Tao, H.W. (2013). Linear transformation of thalamocortical input by intracortical excitation. Nat. Neurosci. *16*, 1324–1330.

Lien, A.D., and Scanziani, M. (2013). Tuned thalamic excitation is amplified by visual cortical circuits. Nat. Neurosci. *16*, 1315–1323.

Liu, B. -h., Li, P., Li, Y. -t., Sun, Y.J., Yanagawa, Y., Obata, K., Zhang, L.I., and Tao, H.W. (2009). Visual Receptive Field Structure of Cortical Inhibitory Neurons Revealed

by Two-Photon Imaging Guided Recording. J. Neurosci. *29*, 10520–10532.

Mangini, N.J., and Pearlman, A.L. (1980). Laminar distribution of receptive field properties in the primary visual cortex of the mouse. J. Comp. Neurol. *193*, 203–222.

Mao, B.-Q., Hamzei-Sichani, F., Aronov, D., Froemke, R.C., and Yuste, R. (2001). Dynamics of Spontaneous Activity in Neocortical Slices. Neuron *32*, 883–898.

Markram, H., Helm, P.J., and Sakmann, B. (1995). Dendritic calcium transients evoked by single back-propagating action potentials in rat neocortical pyramidal neurons. J. Physiol. *485 (Pt 1*, 1–20.

Marshel, J.H., Kaye, A.P., Nauhaus, I., and Callaway, E.M. (2012). Anterior-Posterior Direction Opponency in the Superficial Mouse Lateral Geniculate Nucleus. Neuron *76*, 713–720.

Metin, C., Godement, P., and Imbert, M. (1988). The primary visual cortex in the mouse: Receptive field properties and functional organization. Exp. Brain Res. *69*, 594–612.

Murayama, M., Pérez-Garci, E., Nevian, T., Bock, T., Senn, W., and Larkum, M.E. (2009). Dendritic encoding of sensory stimuli controlled by deep cortical interneurons. Nature *457*, 1137–1141.

Nevian, T., and Helmchen, F. (2007). Calcium indicator loading of neurons using single-cell electroporation. Pfl{ü}gers Arch. - Eur. J. Physiol. *454*, 675–688.

Niell, C.M., and Stryker, M.P. (2008). Highly Selective Receptive Fields in Mouse Visual Cortex. J. Neurosci. *28*, 7520–7536.

Niell, C.M., and Stryker, M.P. (2010). Modulation of Visual Responses by Behavioral State in Mouse Visual Cortex. Neuron *65*, 472–479.

Nikonov, S.S., Kholodenko, R., Lem, J., and Pugh, E.N. (2006). Physiological Features of the S- and M-cone Photoreceptors of Wild-type Mice from Single-cell Recordings. J. Gen. Physiol. *127*, 359–374.

Ohki, K., and Reid, R.C. (2007). Specificity and randomness in the visual cortex. Curr. Opin. Neurobiol. *17*, 401–407.

Ohki, K., Chung, S., Ch'ng, Y.H., Kara, P., and Reid, R.C. (2005). Functional imaging

with cellular resolution reveals precise micro-architecture in visual cortex. Nature *433*, 597–603.

Olshausen, B.A., and Field, D.J. (2004). Sparse coding of sensory inputs. Curr. Opin. Neurobiol. *14*, 481–487.

Palmer, L.M., Schulz, J.M., Murphy, S.C., Ledergerber, D., Murayama, M., and Larkum, M.E. (2012). The cellular basis of GABA(B)-mediated interhemispheric inhibition. Science (80-.). *335*, 989–993.

Palmer, L.M., Shai, A.S., Reeve, J.E., Anderson, H.L., Paulsen, O., and Larkum, M.E. (2014). NMDA spikes enhance action potential generation during sensory input. Nat. Neurosci. *17*, 383–390.

Pelli, D.G. (1997). The VideoToolbox software for visual psychophysics: transforming numbers into movies. Spat. Vis. *10*, 437–442.

Pérez-Garci, E., Larkum, M.E., and Nevian, T. (2013). Inhibition of dendritic Ca2+ spikes by GABAB receptors in cortical pyramidal neurons is mediated by a direct Gi/o-β-subunit interaction with Cav1 channels. J. Physiol. *591*, 1599–1612.

Piscopo, D.M., El-Danaf, R.N., Huberman, A.D., and Niell, C.M. (2013). Diverse Visual Features Encoded in Mouse Lateral Geniculate Nucleus. J. Neurosci. *33*, 4642–4656.

Polsky, A., Mel, B.W., and Schiller, J. (2004). Computational subunits in thin dendrites of pyramidal cells. Nat. Neurosci. *7*, 621–627.

Potez, S., and Larkum, M.E. (2008). Effect of common anesthetics on dendritic properties in layer 5 neocortical pyramidal neurons. J. Neurophysiol. *99*, 1394–1407.

Priebe, N.J., and McGee, A.W. (2014). Mouse vision as a gateway for understanding how experience shapes neural circuits. Front. Neural Circuits *8*, 123.

Rall, W.R. (1964). Theoretical significance of dendritic trees for neuronal input-output relations. In Neural Teory and Modeling (Reiss RF, Ed.), (Stanford University Press), pp. 73–97.

Raz, A., Grady, S.M., Krause, B.M., Uhlrich, D.J., Manning, K.A., and Banks, M.I. (2014). Preferential effect of isoflurane on top-down vs. bottom-up pathways in sensory cortex. Front. Syst. Neurosci. *8*, 191.

Ringach, D.L., Shapley, R.M., and Hawken, M.J. (2002). Orientation selectivity in macaque V1: diversity and laminar dependence. J. Neurosci. *22*, 5639–5651.

Rivlin-Etzion, M., Zhou, K., Wei, W., Elstrott, J., Nguyen, P.L., Barres, B.A., Huberman, A.D., and Feller, M.B. (2011). Transgenic Mice Reveal Unexpected Diversity of On-Off Direction-Selective Retinal Ganglion Cell Subtypes and Brain Structures Involved in Motion Processing. J. Neurosci. *31*.

Schiller, J., Schiller, Y., Stuart, G., and Sakmann, B. (1997). Calcium action potentials restricted to distal apical dendrites of rat neocortical pyramidal neurons. J. Physiol. *505*, 605–616.

Schiller, J., Major, G., Koester, H.J., and Schiller, Y. (2000). NMDA spikes in basal dendrites of cortical pyramidal neurons. Nature *404*, 285–289.

Scholl, B., Tan, A.Y.Y., Corey, J., and Priebe, N.J. (2013). Emergence of orientation selectivity in the Mammalian visual pathway. J. Neurosci. *33*, 10616–10624.

Seabrook, T.A., Burbridge, T.J., Crair, M.C., and Huberman, A.D. (2017). Assembly of the Mouse Visual System. Annu. Rev. Neurosci. *40*, 499–538.

Sheffield, M.E.J., and Dombeck, D.A. (2015). Calcium transient prevalence across the dendritic arbour predicts place field properties. Nature *517*, 200–204.

Shepherd, G.M. (1996). The dendritic spine: a multifunctional integrative unit. J. Neurophysiol. *75*, 2197–2210.

Smith, S.L., and Häusser, M. (2010). Parallel processing of visual space by neighboring neurons in mouse visual cortex. Nat. Neurosci. *13*, 1144–1149.

Smith, S.L., Smith, I.T., Branco, T., and Häusser, M. (2013). Dendritic spikes enhance stimulus selectivity in cortical neurons in vivo. Nature *503*, 115–120.

Spencer, W.A., and Kandel, E.R. (1961). Electrophysiology of hippocampal neurons: IV. Fast prepotentials. J Neurophysiol *24*, 272–285.

Spruston, N., Häusser, M., and Stuart, G. (2013). Chapter 11 – Information Processing in Dendrites and Spines. In Fundamental Neuroscience, pp. 231–260.

Steriade, M. (2001). Impact of network activities on neuronal properties in corticothalamic systems. J. Neurophysiol. *86*, 1–39.

Stosiek, C., Garaschuk, O., Holthoff, K., and Konnerth, A. (2003). In vivo two-photon calcium imaging of neuronal networks. Proc. Natl. Acad. Sci. U. S. A. *100*, 7319–7324.

Stuart, G.J., and Spruston, N. (2015). Dendritic integration: 60 years of progress. Nat. Neurosci. *18*, 1713–1721.

Stuart, G., Schiller, J., and Sakmann, B. (1997). Action potential initiation and propagation in rat neocortical pyramidal neurons. J. Physiol. *505*, 617–632.

Stuart, G.J., Dodt, H.U., and Sakmann, B. (1993). Patch-clamp recordings from the soma and dendrites of neurons in brain slices using infrared video microscopy. Pflugers Arch. *423*, 511–518.

Sun, W., Tan, Z., Mensh, B.D., and Ji, N. (2015). Thalamus provides layer 4 of primary visual cortex with orientation- and direction-tuned inputs. Nat. Neurosci. *19*, 308–315.

Swindale, N. V (1998). Orientation tuning curves: empirical description and estimation of parameters. Biol. Cybern. *78*, 45–56.

Szél, Á., Röhlich, P., Gaffé, A.R., Juliusson, B., Aguirre, G., and Van Veen, T. (1992). Unique topographic separation of two spectral classes of cones in the mouse retina. J. Comp. Neurol. *325*, 327–342.

Szél, Á., Röhlich, P., Mieziewska, K., Aguirre, G., and van Veen, T. (1993). Spatial and temporal differences between the expression of short- and middle-wave sensitive cone pigments in the mouse retina: A developmental study. J. Comp. Neurol. *331*, 564–577.

Tamás, G., Szabadics, J., and Somogyi, P. (2002). Cell type- and subcellular position-dependent summation of unitary postsynaptic potentials in neocortical neurons. *22*.

Tischbirek, C., Birkner, A., Jia, H., Sakmann, B., and Konnerth, A. (2015). Deep two-photon brain imaging with a red-shifted fluorometric Ca2+ indicator. Proc. Natl. Acad. Sci. U. S. A. *112*, 11377–11382.

Vaiceliunaite, A., Erisken, S., Franzen, F., Katzner, S., and Busse, L. (2013). Spatial integration in mouse primary visual cortex. J. Neurophysiol. *110*.

Valverde, F. (1968). Structural changes in the area striata of the mouse after enucleation. Exp. Brain Res. *5*, 274–292.

Vaney, D.I., Sivyer, B., and Taylor, W.R. (2012). Direction selectivity in the retina: symmetry and asymmetry in structure and function. Nat. Rev. Neurosci. *13*, 194–208.

Varga, Z., Jia, H., Sakmann, B., and Konnerth, A. (2011). Dendritic coding of multiple sensory inputs in single cortical neurons in vivo. Proc. Natl. Acad. Sci. U. S. A. *108*, 15420–15425.

Villeneuve, M.Y., and Casanova, C. (2003). On the use of isoflurane versus halothane in the study of visual response properties of single cells in the primary visual cortex. J. Neurosci. Methods *129*, 19–31.

Vlasits, A.L.L., Bos, R., Morrie, R.D.D., Fortuny, C., Flannery, J.G.G., Feller, M.B.B., and Rivlin-Etzion, M. (2014). Visual Stimulation Switches the Polarity of Excitatory Input to Starburst Amacrine Cells. Neuron *83*, 1172–1184.

Wagor, E., Mangini, N.J., and Pearlman, A.L. (1980). Retinotopic organization of striate and extrastriate visual cortex in the mouse. J. Comp. Neurol. *193*, 187–202.

Waters, J., Larkum, M., Sakmann, B., and Helmchen, F. (2003). Supralinear Ca2+ influx into dendritic tufts of layer 2/3 neocortical pyramidal neurons in vitro and in vivo. J. Neurosci. *23*, 8558–8567.

Wertz, A., Trenholm, S., Yonehara, K., Hillier, D., Raics, Z., Leinweber, M., Szalay, G., Ghanem, A., Keller, G., Rozsa, B., et al. (2015). Single-cell-initiated monosynaptic tracing reveals layer-specific cortical network modules. Science (80-.). *349*, 70–74.

Wilson, D.E., Whitney, D.E., Scholl, B., and Fitzpatrick, D. (2016). Orientation selectivity and the functional clustering of synaptic inputs in primary visual cortex. Nat. Neurosci. *19*, 1003–1009.

van Wyk, M., Wässle, H., Taylor, W.R., and Michiel Van Wyk, Heinz Wässle, W.R.T. (2009). Receptive field properties of ON- and OFF-ganglion cells in the mouse retina. Vis. Neurosci. *26*, 297–308.

Xu, N., Harnett, M.T., Williams, S.R., Huber, D., O'Connor, D.H., Svoboda, K., and Magee, J.C. (2012). Nonlinear dendritic integration of sensory and motor input during an active sensing task. Nature *492*, 247–251.

Yang, T., and Maunsell, J.H. (2004). The effect of perceptual learning on neuronal responses in monkey visual area V4. J. Neurosci. *24*, 1617–1626.

Yuste, R. (2013). Electrical Compartmentalization in Dendritic Spines. Annu. Rev. Neurosci. *36*, 429–449.

Yuste, R., and Denk, W. (1995). Dendritic spines as basic functional units of neuronal integration. Nature *375*, 682–684.

Zhao, X., Chen, H., Liu, X., and Cang, J. (2013). Orientation-selective Responses in the Mouse Lateral Geniculate Nucleus. J. Neurosci. *33*, 12751–12763.

Zhu, J.J., and Connors, B.W. (1999). Intrinsic firing patterns and whisker-evoked synaptic responses of neurons in the rat barrel cortex. J. Neurophysiol. *81*, 1171–1183.

Zorec, R., Araque, A., Carmignoto, G., Haydon, P.G., Verkhratsky, A., and Parpura, V. (2012). Astroglial Excitability and Gliotransmission: An Appraisal of Ca^{2+} as a Signalling Route. ASN Neuro *4*, AN20110061.

6 Acknowledgements

At the time of writing this thesis, I want to express my deepest gratitude to my advisor, Prof. Dr. Arthur Konnerth. He has been generously providing me with support, guidance, encouragement and most importantly a world-class research environment.

I would like to thank my thesis mentors, Prof. Dr. Helmuth Adelsberger and Prof. Dr. Markus Ploner, for their invaluable support and advice. Prof. Dr. Helmuth Adelsberger as a member of the lab has been taking care of all the experimental procedures and ensured a trouble-free running of the lab.

I also want to thank Dr. Valérie Bonfardin who taught me many things when I started working in the lab. We spent a lot of time investigating the function of interneurons in visual cortex and during this time I gained a lot of experience.

I am very glad that I started the spine imaging project with Dr. Beomjong Song who spent a lot of effort in improving the recording. I also like to thank Dr. Tatsuo Sato who provided so many useful suggestions on the project. He joined the project in the later phase and offered me a lot of advice and guidance on data analysis and thesis writing.

Thanks to the wonderful two-photon microscope built by Dr. Hongbo Jia, I could perform those amazing experiments. Dr. Jia as a senior colleague also offered a lot of help and advice.

I am very thankful that I am working with those great colleagues. Antje Birkner and Carsten Tischbirek made a nice technical development on deep imaging which was very useful for my project. Antje particularly helped me with the translation of the abstract. Yonghai Zhang, Hsing-Jung Chen, Arjan Dijke and Dr. Takahiro Noda also provided a lot of help during my thesis writing.

I also deeply appreciate the help during my study in the lab from our technical staff, Felix Beyer, Christian Obermayer, Christine Karrer, Dr. Rosa Maria Karl, Andreas Fohr and Petra Apostolopoulos.

At last, I want to express my deepest gratitude again to my parents for their constant support and encouragement over the past 30 years.

7 Publications

Chen Y, Zhang Y, Song B, Sato T, Obermayer C, Jia H and Konnerth A. (2017). Layer 1 inputs regulate visual processing in cortical layer 4. *In submission.*